NUCLEOSOMAL ARRAYS: A NOVEL METHOD TO DETECT PD-L1 ON THE CELL SURFACE

A thesis presented in partial fulfilment of the requirements for the degree of
Master of Science
in
Biochemistry
at Massey University, Palmerston North,
New Zealand.

Aseel Mohammad

2021

Abstract

Cancer is a complex group of diseases that can be difficult to therapeutically target as cancer cells develop a myriad of mechanisms to spread and survive. Immune evasion is one such mechanism cancer cells use to bypass the immune system and continue to invade other tissues. Evading the immune system is achieved through over-expression of the immune checkpoint protein programmed death ligand-1 (PD-L1). This protein is used as a predictive bio-marker to determine whether cancer patients are viable for PD-L1 immunotherapy, and over-expression of PD-L1 is determined using immunohistochemistry assays. Given that these assays use different PD-L1 antibodies that recognise different epitopes, it introduces variability to staining patterns and scoring matrices. This study has taken advantage of the endogenous high affinity interaction between PD-L1 and its receptor, programmed death receptor-1 (PD-1), to create a novel technique to detect PD-L1 on the surface of cancer cells. Nucleosomal arrays were formed with PD-1 peptide tagged to histone H2B containing octamers and fluorescently labelled DNA. These nucleosomal assemblies had correct nucleosome formation when using biotin-labelled positioning DNA and were able to be detected by binding Avidin-Alexa 488. These nucleosomal arrays bound specifically to PD-L1 on the surface of cancer cells shown by fluorescent confocal microscopy and demonstrated greater specificity than Wild Type H2B containing nucleosomal arrays. The use of nucleosomal arrays in this manner has an advantage over an antibody as there are a greater number of PD-L1 binding sites, and the fluorescent signal is able to be amplified due to positioning DNA being labelled at multiple sites. Though this study used the PD-L1/PD-1 interaction as a proof of principle, other short specific binding domains could be attached to the N-terminal tail of histones that could detect other extracellular proteins. This novel detection method is efficient and specific, and further optimisation in other fluorescent

detection platforms may yield a more consistent and high-throughput method to detect extracellular proteins to determine patient response to immunotherapy treatments.

COVID-19 Statement

Due to COVID-19 and the resulting university closure in 2020 that meant lack of laboratory access for 2 months, the stated objectives and experiments were unable to be completed. These experiments included TEM imaging of PD-1/H2B nucleosomal arrays (see Chapter Section **3.3**), and FACS analysis of PD-1/H2B and WT nucleosomal arrays (see Chapter Section **4.3**). Due to the lack of time to optimise these experiments, aim 3 (see Introduction Section **1.5**) was unable to be completed in full.

Acknowledgements

In the name of Allah, the most Gracious and the most Merciful,

I would firstly like to thank my supervisors Dr. Jeong Park and Dr. Tracy Hale. Dr. Jeong Park provided me vital foundations for the beginning of my research. Dr. Tracy Hale always had her door open whenever I had any questions (even the unintelligent ones) and her valuable insight was a great help to me during the most uncertain times in my research.

To all my friends in the science department which have lifted my spirits by encouragement and procrastination, I thank you.

To Faye, Emma, Ann, Devon, Jayde, and Emily, thank you for keeping me sane and entertained.

I would also like to thank my father Fidel, my mother Ibtisam, my sisters Haneen, Naheel and Hadeel, and Jeopardy for supporting me throughout the entirety of my studies.

Abbreviations

Am	Ampicillin
Chl	Chloramphenicol
BSA	Bovine Serum Albumin
cDNA	Complementary Deoxyribonucleic Acid
DMEM	Dulbecco's Modified Eagle Medium
DMSO	Dimethyl Sulfoxide
DNase	Deoxyribonuclease
E. coli	*Escherichia coli*
EDTA	Ethylene Diamine Tetraacetic Acid
EtBr	Ethidium Bromide
EtOH	Ethanol
FBS	Fetal Bovine Serum
GUSB	β-Glucuronidase
H1299	Human Non-small Cell Lung Carcinoma cell line
HeLa	Human Cervical Adenocarcinoma cell line
h	Hours
IHC	Immunohistochemistry
Kb	Kilobases
kDa	Kilodalton
LB	Luria Bertani Bacteriological Medium
LN-18	Human Glioblastoma cell line
M	mol/L
mA	Milliamperes
MCF-7	Human Breast Adenocarcinoma cell line
MHC I	Major Histocompatibility Class I
Min	Minutes

mL	Millilitres
MNase	Micrococcal Nuclease
NF-$\varkappa$B	Nuclear Factor Kappa B
NK	Natural Killer
NP-40	Igepal CA-630
PBS	Phosphate Buffered Saline
PCR	Polymerase Chain Reaction
PD-1	Programmed Death Receptor-1
PD-1/H2B	PD-1 Tagged Histone H2B
PD-L1	Programmed Death Ligand-1
PDR	Programmed Death Receptor (attached to H2B)
Pen/Strep	Penicillin-Streptomycin
PMSF	Phenylmethylsulfonyl Fluoride
PVDF	Polyvinylidene Difluoride
qPCR	Quantitative PCR
RCF	Relative Centrifugal Force
RNase	Ribonuclease
RPM	Revolutions Per Minute
RT-qPCR	Reverse Transcription Quantitative PCR
s	Seconds
SDS	Sodium Dodecyl Sulphate
SDS-PAGE	SDS-Polyacrylamide Gel Electrophoresis
TBE	Tris/Boric Acid/EDTA
TBS	Tris Buffered Saline
TBST	Tris-Buffered Saline/Tween-20
TE	Tris EDTA Buffer
TEMED	Tetramethylethylenediamine
Tm	Melting Temperature
U2OS	Human Osteosarcoma cell line
U87-MG	Human Uppsala 87 Malignant Glioma cell line
V	Volts
Vol	Volume

Contents

List of Tables

List of Figures

Chapter 1

Introduction

1.1 Cancer

Each year worldwide, approximately 9.5 million people die of cancer. Cancer not only poses a health risk to individuals, but is also likely to have confounding impacts on a patient's socio-economic welfare and mental health. Cancer can be diagnosed through biopsy, MRI, and X-ray, and treatment is usually dependent on tumour type, malignancy, and tissue source, but can range from surgical resection to radiotherapy and chemotherapy. There is an increasing need for novel treatments to specifically target cancer cells, though this can be difficult due to the multitude of various mutations that can arise in a single tumour. Cancer cells can arise by avoiding death signals and enhancing growth signals, as well as avoiding DNA repair mechanisms. These traits were outlined in the paper by Hanahan and Weinberg (2000). Through these means, tumour cells are able to sustain their proliferative state and become increasingly intrusive within their environment. Emerging hallmarks of cancer have also been recently described such as immune evasion (Hanahan and Weinberg, 2011). This is where cancer cells are able to bypass the immune system by deactivating key immune checkpoint pathways, one of which involves the protein programmed death ligand-1 (PD-L1).

1.2 Immune Evasion

The interaction between the immune system and cancer cells is complex, and this complexity increases the difficulty in developing novel therapeutic drug treatments. Some cancer cells are able to evade the immune system and metastasise within other tissues by deactivating key immune checkpoint pathways to in order to go undetected. Conditions that may facilitate the increased risk of immune evasion by cancer cells are changes due to infection or chronic inflammation and allow cancer cells to undergo what is known as 'immuno-sculpting'. This theory describes how cancer cells are able to go from somatic cells to detectable cancer cells. The theory, as described in the paper by Dunn et al. (2004), details the three stages of this process (Figure 1.1).

In the first stage, cancer cells are eradicated by the immune system provided that they express tumour-specific antigens to be targeted by immune cells such

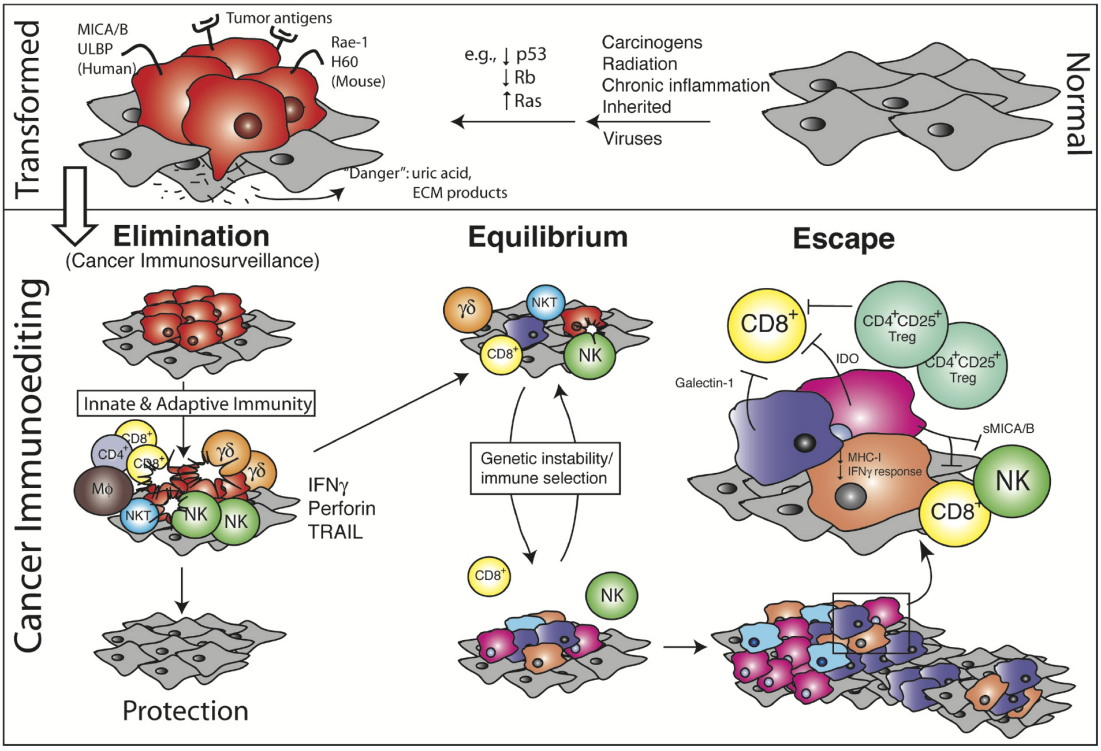

Figure 1.1: The Three Stages of The Immuno-Sculpting Process. Representative image of the three stages of the immuno-sculpting process. (Dunn et al., 2004).

as CD8+ cytotoxic T cells and CD4+ helper T cells. The second stage, known as equilibrium, describes how cancer cells which are not targeted by the immune system lie dormant and have the ability to replicate variants that do not have targetable antigens exposed. These cells may lie dormant for a certain period of time before they re-emerge, or may not re-emerge at all if the patient's immune system is able to target them once more. In the third stage, escape, cancer cells which have not been exposed to the immune system and have formed resistant variants are able to escape the immune system and once again metastasise. This can occur if certain cancer cells are not recognised by the immune system, if there is down-regulation of the immune system, or excess inflammation. It should be noted that even if a patient's immune system is in full working order, it is redundant if the cancer cells are no longer targetable. Regardless, these escaped cells are able to once again excessively replicate and travel to other areas of the body. Thus they have evaded the immune system completely.

The adaptive arm of the immune response is made up of numerous receptors and their ligands, which help regulate antigen recognition within the emerging

immune system and maintain self-tolerance. This occurs through immune checkpoint pathways. During negative T-cell selection, T-cells that attack self-antigens indiscriminately are deactivated or undergo apoptosis in order to prevent disadvantageous auto-immune reactions (Klein et al., 2014; Takaba and Takayanagi, 2017). Naïve T-cells are differentiated into cytotoxic CD8+ cells that function to kill cancer cells, or helper CD4+ T-cells used to fight infections by releasing cytokines used for signalling other immune proteins and pathways (Leonard and Lin, 2000). This is based on major histocompatibility (MHC) class antigens cytokines are presented with (Gutcher and Becher, 2007). This process is facilitated through notable immune checkpoint proteins such as Cytotoxic T lymphocyte-associated molecule-4 (CTLA-4), programmed cell death receptor-1 (PD-1), and programmed cell death ligand-1 (PD-L1).

1.3 PD-L1 Immune Checkpoint Protein

PD-L1, otherwise known as B7 Homolog 1 or CD274, is a 33-40 kDa immune checkpoint protein expressed on the surface of antigen-presenting L and B lymphocytes, a type of white blood cell that makes up part of the immune system. It is a transmembrane glycoprotein part of the immunoglobulin super-family and has characteristic extracellular Ig variable and Ig constant regions, followed by a hydrophobic domain that spans the membrane, and an intracellular domain. It is the variable regions of PD-L1 that interact with its receptor, PD-1, that leads to T-cell exhaustion.

PD-L1 binds to the receptor PD-1, expressed on the surface of T cells and selectively on Natural Killer (NK) cells to suppress the immune response (Butte et al., 2007; Wang et al., 2016). PD-L1 binding to its receptor, PD-1, results in deactivation of T-cells through the phosphorylation of two tyrosine residues within the immunoreceptor tyrosine-based inhibitory motif (ITIM) located within the cytoplasmic domain of PD-1 (Parry et al., 2005; Yokosuka et al., 2012). The tyrosine-based inhibitory motif is found within immune system receptors in order to attenuate cell signalling during immune cell activation (Barrow and Trowsdale, 2006). Phosphorylation of the tyrosine residues may be through the action

of lymphocyte-specific protein kinase (Lck) or C-terminal src-kinase but the specific mechanism is as yet unclear (Sheppard et al., 2004). This then deactivates the T-cell antigen receptor (TCR) leading to T-cell apoptosis (Parry et al., 2005; Yokosuka et al., 2012).

The PD-L1 activation pathway is complex and recruits numerous transcription factors and kinases in order regulate PD-L1 expression. PD-L1 expression is stimulated by Interferon-γ (IFN-γ) and nuclear factor kappa light chain enhancer of activated B cells (NF-$\varkappa$B) (Gowrishankar et al., 2015). IFN-γ is a pro-inflammatory cytokine produced by NK cells and is a class II MHC molecule. Binding to its receptors IFNγ Receptors 1 and 2 activates Janus kinase (JAK) and signal transducer and activator of transcription (STAT) pathway in order activate interferon regulatory factor 1 (IRF1) which then binds to the PD-L1 promoter region to bring about its transcription. The JAK-STAT pathway is also able to recruit transcriptions factors such as MYC and NF-$\varkappa$B which are able to bind to the promoter region of PD-L1 (Garcia-Diaz et al., 2017; Moon et al., 2017). NF-$\varkappa$B is a transcription factor involved in cell survival and proliferation. It exists in an inactive state in the cell until its activation is bought about by I$\varkappa$B Kinase. In cancer cells, NF-$\varkappa$B is found to be constitutively active and enhances the expression of genes needed for survival and proliferation, and is an inhibitor of cellular apoptosis (Taniguchi and Karin, 2018).

PD-L1 over-expression has been found in a variety of cancer states including glioblastoma (Berghoff et al., 2015; Xue et al., 2017), renal cell carcinoma (Thompson et al., 2006), non-small cell lung carcinoma (Pawelczyk et al., 2019), and urothelial carcinoma (Nakanishi et al., 2007). Over-expression of PD-L1 is linked to poor cancer patient prognosis, particularly in the case of glioblastoma cancer patients (Hao et al., 2020). Glioblastoma multiform (GBM) is an aggressive grade VI brain tumour, whose patient survival is only expected to be 12-15 months after diagnosis (Alifieris and Trafalis, 2015; Tang et al., 2019). It can often be difficult to target these tumours due to the blood-brain barrier, and the location of the tumour in the brain. Other studies have reported that over-expression of PD-L1 is correlated with positive patient prognosis, and increased chance of survival thus indicating the unpredictable nature of the signalling pathway (Gato-Cañas et al., 2017). Studies conducted on different tumours have used PD-L1 expression levels as a predictive bio-marker to determine not only patient prognosis, but also

patient response to drugs targeting PD-L1. If a patient has undergone a PD-L1 expression test, they may be viable to undergo therapy with either PD-L1 or PD-1 antibodies. Patients are able to undergo a PD-L1 IHC (immunohistochemistry) diagnostic assay in order to determine whether they are viable for antibody therapy.

1.4 Immunohistochemistry assays

Immune evasion of cells is a relatively recent hallmark of cancer that emerged after well regarded characteristics such as evasion of death signals, and promotion of growth enhancers. In order to suppress immune evasion of tumours in cancer patients, pharmaceutical companies have developed PD-L1 and PD-1 therapies that utilize antibodies that target the receptor-ligand interaction. IHC is utilized to assess patient viability for PD-L1/PD-1 therapies (Diggs and Hsueh, 2017). Those patients who exhibit over-expression of PD-L1 in tumour cells are recommended treatment.

IHC assays are used to determine the expression levels of an antigen in a patient tissue sample using predictive bio-markers as targets. IHC staining involves incubating a formaldehyde-fixed patient sample with a primary antibody: an antibody that binds to the epitope of interest. This first antibody is then detected by a secondary antibody that is tagged with horseradish peroxidase (HRP) or Alkaline Phosphatase (AP). A chromogen such as 3,3'-diaminobenzidine (DAB) reacts with the tag to produce a red-brown coloured reaction that is able to be visualised. Brown deposits are indicative of positive staining (Ramos-Vara and Miller, 2014). However, IHC assays are not quantitative unlike those utilizing fluorophores where fluorescence can be measured.

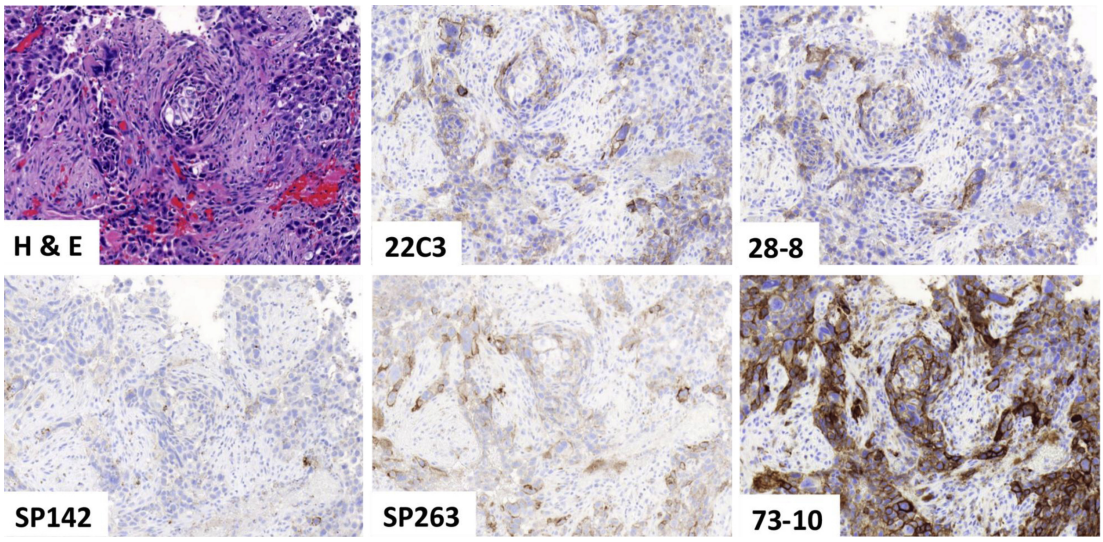

Figure 1.2: PD-L1 Antibody Staining. Representative PD-L1 staining using five commonly used PD-L1 antibodies used in commercially available IHC assays. H & E, haematoxylin and eosin staining. (Tsao et al., 2018).

There are a variety of IHC diagnostic kits available, each with their own detection antibody and specific scoring matrix. Each assay uses a specific splicing variant, some of which are used for both detection and therapeutics. However, it has become increasingly clear that there is lack of consistency between different IHC kits (Kintsler et al., 2019). IHC standardisation can be hard to maintain, especially between laboratories which have their own scoring criteria for patient samples, and different staining protocols which can affect the outcome of a diagnostic assay. Two laboratories conducting IHC assays on the same patient samples may score them differently such that one lab may determine a patient needs a specific drug or therapy to target the protein or antigen of interest, while an alternative lab may determine that the patient sample falls below their threshold for therapy. This can compromise the health of the patient if they do not receive the treatment they need. PD-L1 IHC assays are one example of how these standardisation problems can severely affect a patient. Concerns have also been raised about the sensitivity of each antibody used in each assay. Figure 1.2 shows that using different antibodies results in different staining intensities. Antibodies 22C3, SP263 and 28-8 have comparable staining patterns, whereas others such as 73-10 show much higher sensitivity to PD-L1. This indicates that only certain PD-L1 antibodies are inter-changeable, but laboratories will only use one PD-L1 antibody for IHC staining. It is apparent that a universal improved

diagnostic reagent is needed in order to determine whether patients are viable for PD-L1/PD-1 therapy.

Currently there are six antibodies that have been FDA approved for patients requiring PD-L1/PD-1 therapy. These are described in Table 1.1. All therapies share one common goal: to inhibit the interaction between PD-L1 on tumour cells and PD-1 on T cells, thereby allowing the body to target the malignant cells via other means such as NK cells that target tumour cells lacking MHC I molecules. Increased levels of NK cells within tumour sites have lead to positive outcomes (Marcus et al., 2014; Coca et al., 1997).

Therapy Agent	**Year**	**Target**	**Oncogenic States**
Permbrolizumab	2014	PD-1	Melanoma NSCLC
Nivolumab	2014	PD-1	Melanoma Squamous cell lung cancer Renal cell carcinoma Hodgkin's lymphoma Urothelial carcinoma
Atezolizumab	2016	PD-L1	Urothelial carcinoma Triple negative breast cancer NSCLC
Avelumab	2017	PD-L1	Merkel cell carcinoma NSCLC
Durvalumab	2017	PD-L1	Urothelial carcinoma NSCLC Head and neck cancer
Cemiplimab	2018	PD-1	Myeloma Squamous cell skin cancer Lung cancer

Table 1.1: PD-1/PD-L1 Therapy Agents. Each agent is listed along with the associated oncogenic states its use has been approved for in trials. NSCLC, non-small cell lung cancer, * - this agent failed its phase 3 trial in bladder cancer in 2017.

Recent studies have also shown that combinatorial therapy using different treatments for checkpoint inhibition is more favourable than a single treatments. Ipilimumab is a monoclonal antibody that targets CTLA-4 that down-regulates immune response much like PD-L1 (Buchbinder and Desai, 2016). In the case of melanoma and NSCLC patients, the most common combination is Nivolumab and Ipilimumab. Melanoma patients treated with both treatments had a median progression-free survival time of 11.5 months compared to the individual Nivolumab group (6.9 months) and the Ipilimumab group (2.9 months), supports

use of multiple agents to target aspects of immune evasion as a treatment option (Hodi et al., 2018).

1.5 Chromatin

In order to fit all the information contained within the nucleus, cells condense their DNA into a universal packaging system called chromatin. In 1974, Kornberg published his seminal paper "Chromatin Structure: A Repeating Unit of Histones and DNA" that detailed how DNA within the nucleus is compacted into repeating units called nucleosomes which are made up of approximately 147 bp of DNA wound around an octamer of histone proteins. An octamer contains two units of histones H2A, H2B, H3, and H4, in which H2A and H2B form two dimers, and H3 and H4 form a tetramer. Linker DNA approximately 80 bp is found between the repeating octamer units, though this length depends on species. Repeating nucleosomes thus make up a 10 nm nucleosome fibre. This fibre is often described as a 'beads on a string' structure (Baldi et al., 2020). Further compaction due to super-coiling turns this 10 nm into a 30 nm fibre requiring a fifth histone, linker histone H1. Higher orders of folding eventually result in the DNA compacted into a chromosome. When cells are in interphase, chromatin can be separated into highly compacted and gene suppressing heterochromatin, and loosely compacted euchromatin that allows transcription factors to access genes. Domains regulated by proteins interact with and modify histones to determine gene expression. The ability of enzymes and proteins to access these areas is high regulated through various means of chromatin regulator proteins such as heterochromatin protein 1, as well as chemical alterations to histone protein tails.

1.5.1 Histone Structure

Histone proteins range in molecular weight from approximately 11 kDa to 15 kDa, with histone H4 being the smallest histone. All contain a characteristic histone fold domain that is made up of a combination of three α-helices connected by two loops (Arents and Moudrianakis, 1995). Additionally, histone proteins contain an unstructured N and C terminal tails that contribute significantly to nucleosome

stability through the action of post-translational modifications, particularly the N-terminal tail (Ng et al., 2009). Furthermore, these tails protrude from the core nucleosome structure which allows them to be targeted by modifying enzymes that modulate gene expression. The combination of post-translational modification and their reversibility is what makes up the epigenetic code, and allows for differential gene expression. The N-terminal tails of histones are a highly conserved feature and can be found in many different organisms ranging from yeast to humans. However, these N-terminal tails contain no structured domains, and hence their ability to regulate gene expression comes from post-translational modifications such as acetylation and methylation (Bannister and Kouzarides, 2011). These chemical changes to residues within histone tails allows them to be more or less compacted to the overall nucleosome structure. More compaction means histones are wound tighter around the DNA. This prevents transcription factors from being able to access the DNA, and thus gene expression is repressed. Modifications such as acetylation decreases the negative charge on histone tails, reducing the electrostatic interaction between them and negatively charged phosphate groups of DNA (Morales and Richard-Foy, 2000).

Though each histone is highly conserved in nature, there are variants that exist in other species, as well as different isoforms that act as substitues for core histone proteins. Specific histones are required for transcription activation or repression, and histones are interchanged through a variety of means, but usually through the action of ATP-dependent chromatin remodellers such as SWI/SNF (Tang et al., 2010). Gene expression modulation through the action of nucleosome positioning and histone exchange determines how available DNA is for transcription. An example of this is histone variant H2A.Z, a variant of histone H2A. Studies have shown that this variant is involved in both transcriptional activation and repression, a unique characteristic unlike other histone variants, but also has other roles in DNA repair, differentiation, and T-cell formation (Rudnizky et al., 2016; Giaimo et al., 2019).

Histone proteins can be easily expressed in an *E.coli* system and purified from bacterial inclusion bodies which are protein aggregates that contain a high concentration of the histones. Inclusion bodies undergo ion exchange chromatography and are unfolded using unfolding buffer containing guanidinium hydrochloride, after which they are subjected to further ion exchange chromatography. Fractions of

interest are pooled and dialysed against distilled water and purified histones can then be reconstituted into histone octamers via dialysis in urea refolding buffer (Rogge et al., 2013; Kintsler et al., 2019). The N-terminal tails of histones are exposed on the outside of the nucleosome and their unstructured nature provides a scaffold for attachment of desired ligands without adversely affecting nucleosome structure (de la Barre et al., 2001).

1.5.2 Nucleosomal Array Structure

In order to make nucleosomal arrays, a nucleosome positioning sequence is used in order to help orientate histone octamers into correct positioning (approximately 200 bp between each nucleosome). A nucleosome positioning sequence is the localisation of DNA relative to the histone octamer. *In vivo*, there are sequences which favour nucleosome assembly at a certain length of DNA, and these sequences act to stabilise the entire nucleosome. This stability determines how likely a nucleosome is adverse to change depending on the conditions and stimuli it experiences. The more nucleosome positioning sequences that are available, the more repeating monomers are able to be formed (the number of repeating units are known as mers). Any length of nucleosomal arrays are able to be formed, including mono, di, and tri-nucleosomal arrays. Producing nucleosomal arrays *in vitro* requires DNA and histone octamers. Nucleosome positioning is a dynamic process, and there are many different *in vitro* sequences available for nucleosome structural studies. The most famous of these is the non-endogenous Widom 601 sequence formed by Widom and colleagues in 1998 (Lowary and Widom, 1998). This sequence is made up of approximately 220 bp, of which 147 bp form the high affinity binding site for octamers. This core sequence is flanked by two linker sequences either side for additional nucleosomes. There are other variations of this sequence such as 601.2 which is 174 bp and incorporates a restriction site, and other sequences such as the 5s rDNA sequence, a 260 bp sequences isolated from the 5s ribosomal RNA gene of *Lytechinus variegatus*.

The Widom 601 nucleosome positioning sequence shown in Figure 1.3 was founded using systematic evolution of ligands by exponential enrichment (SELEX). A random pool of chemically synthesised DNA fragments were tested for their affinity to bind histone octamers. Fragments that had high affinity for octamers were

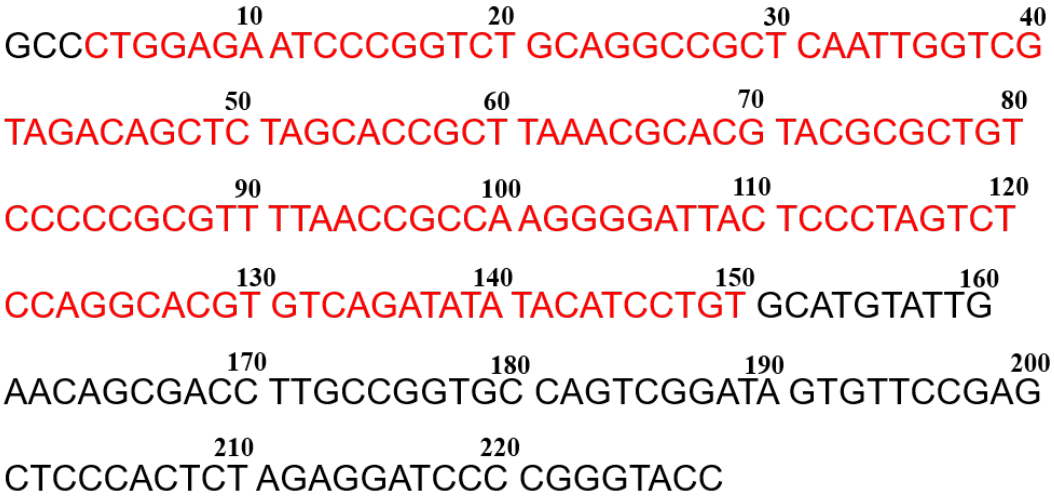

Figure 1.3: Widom 601 Nucleosome Positioning Sequence. The Widom 601 nucleosome positioning sequence, founded using SELEX experiments, is made up of approximately 220 bp. Bases shown in red are used to position the histone octamer with 78 bp of linker DNA leading to the next nucleosome positioning sequence.

cloned, sequenced and tested for their ability to form nucleosomes. From this, the Widom 601 sequence was founded. DNA and histone octamer titrations are needed in order to determine what the correct molar ratios are to make a correctly spaced array, and this is also determined by the assembly method used. The first method of nucleosomal array assembly involves dialysing the assembly in progressively lower concentrations of salt buffer ranging from 1 M salt to 150 mM salt in order to promote DNA-octamer interaction. The second method involves making the assembly and progressively adding dilution buffer to the assembly reaction mixture in order to dilute the salt (Flaus, 2011).

In this study, the extracellular domain of PD-1 receptor (amino acids 118-139) was attached to the end of the N-terminal tail of histone H2B in order to target PD-1/H2B nucleosomal arrays to PD-L1 expressed on the surface of cancer cells. This histone was chosen as the H2A-H2B dimers are found on the surface of the histone octamer, rather than the H3-H4 tetrameric core as shown in Figure 1.4 (Arents et al., 1991). A pUC19 plasmid containing 16 repeats of the Widom 601 nucleosome positioning sequence (16 mer) will be used and optimised to be fluorescently detected. The nucleosomal arrays formed in this study will have 32 binding sites available to bind to PD-L1. As the nucleosomes are identical repeating units, this will provide better specificity of binding to PD-L1 compared to an

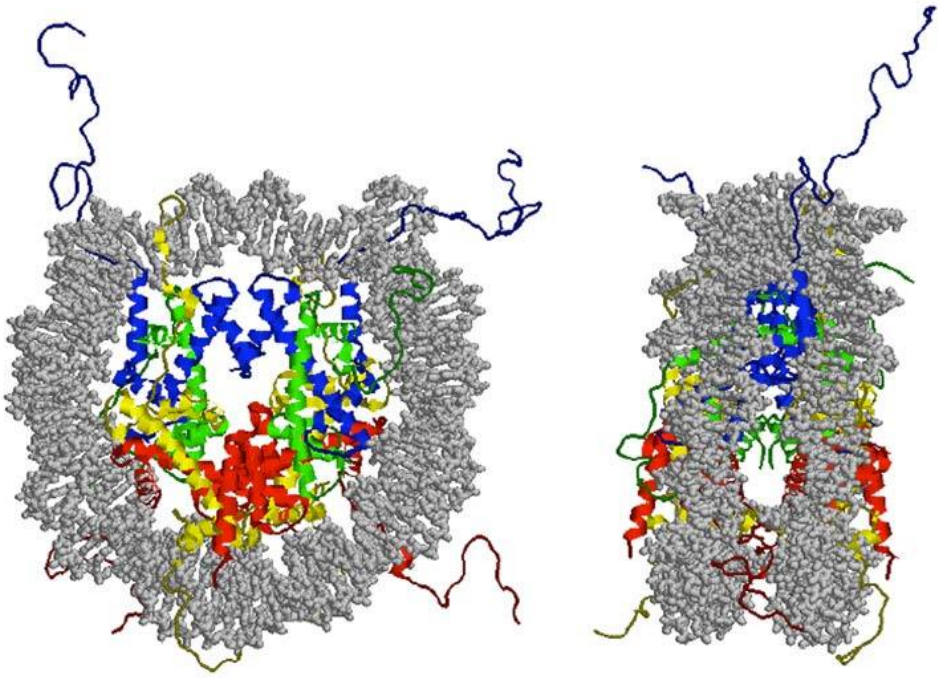

Figure 1.4: Nucleosome Core Particle Structure at 2.8Å Luger structure of the nucleosomal core particle at 2.8 Å The DNA double helix is wound 1.65 times around the histone octamer core. Two copies of each histone are shown inside the nucleosome as red, yellow, blue, and green. N-terminal tails of the histone octamer core are shown outside the nucleosome particle. This figure is adapted from Luger et al. (1997).

antibody that contains two epitope binding sites. As the nucleosome positioning DNA will also be fluorescently detected, this will allow signal amplification so that nucleosomal arrays can be easily detected on the cell surface. Nucleosomal arrays are able to be efficiently made *in vitro*, are cost-effective to create, and are easily modifiable due to the nature of the unstructured histone tails.

1.6 Objectives

Due to the inconsistency in scoring matrices in determining PD-L1 expression levels in patient tumour samples, it is evident that a new reliable diagnostic technique is needed to help patients determine whether they are viable for PD-L1 immunotherapy. To our knowledge, no one has attempted to use nucleosomal arrays as an effective method for detecting extracellular proteins.

We hypothesise that forming a nucleosomal array with a PD-1 derived peptide onto a core histone N-terminal tail and fluorescently detectable DNA is an effective novel diagnostic technique for detecting PD-L1 on cancer cells.

The aims of this study are to:

1. To create nucleosomal arrays with PD-1 peptide octamers and labelled DNA.
    (a) Purify histones and assemble into octamers.
    (b) Fluorescently detect nucleosome positioning DNA.
2. To test binding of nucleosomal arrays.
3. Comparison of nucleosomeal arrays to diagnostic PD-L1 antibody.
    (a) Stain cells with both nucleosomal arrays and with PD-L1 diagnostic antibody.

Chapter 2

Materials and Methods

2.1 Tissue Culture Methods

2.1.1 Cell Line Maintenance

U87-MG, LN18, U2OS, MCF-8, H1299, and HeLa cells were grown at 37°C in 5% CO2 in 100 mm plates in Dulbecco's Modified Eagle Medium (DMEM) supplemented with 10% v/v Foetal Bovine Serum (FBS) and 0.5% penicillin-streptomycin. Cells were passaged approximately every 3-5 days. Prior to passage, growth medium (DMEM) and 0.05% v/v Trypsin/EDTA were warmed at 37°C. Old growth medium was removed from the plates, which were then washed with 10 mL of PBS (137 mM NaCl, 2.7 mM KCl, 10 mM Na2HPO4, 1.8 mM KH2PO4, pH 7.4). After removal, cells were treated with 1 mL of Trypsin/EDTA which was then immediately removed. Cells were incubated for approximately 1-2 minutes, after which cells were dislodged by gently tapping on the plates. Dislodged cells were then resuspended in growth medium at a 1:16 dilution factor.

2.2 RNA Extraction

U87-MG, LN18, U2OS, MCF-7, H1299, and HeLa cells were grown to 80% confluency and the growth medium removed. Cells were washed and scraped with 1 mL PBS, after which they were centrifuged at 3000 rpm for 5 minutes at 4°C. Supernatant was discarded and the cell pellet was resuspended in 800 µL of PBS. From this cell suspension, 100 µL was taken out and placed in a separate tube, to which 300 µL of TRIzol® was added. RNA was then extracted using the Direct-zol™ RNA MiniPrep kit (ZymoResearch). RNA was quantified using the DeNovix DS-11 Spectrophotometer.

2.3 RT-qPCR

Real-time quantitative polymerase chain reaction (RT-qPCR) was performed using RNA extracted from U87-MG, LN18, U2OS, MCF-7, H1299, and HeLa cells

(see Section **2.2**. Extracted RNA was reversely transcribed to cDNA using the SensiFAST™ SYBR® No-ROX One-Step Kit (Bioline) using primers provided by QAIGEN (PD-L1: QT00082775, GUSB: QT00046046). RT-qPCR data was obtained using Roche 480 Lightcycler software. The program was set as follows: 1 cycle at 95°C with a 5 minute hold followed by 12 cycles at 37°C with a 5 second hold. Fluorescence readings were only taken during the 12 cycle period.

2.4 Protein Extraction

Cells were grown to 80-100% confluency before the growth media was removed and cells were washed with 1 mL of PBS before being scraped from each plate. Cells were then centrifuged at 600g for 5 minutes at 4°C before washing once with PBS. Cell were centrifuged again and cell pellets were resuspended in 500 µL RIPA buffer (150 mM Nacl, 1% Igepal CA-630, 0.5% DOC, 0.1% SDS, 50 mM Tris pH 8.0, 1 cOmplete™ ULTRA Mini Protease Cocktail Inhibitor tablet) and incubated on ice for 30 minutes. Cell lysates were then centrifuged at 14000 xg for 10 minutes at 4°C and the supernatant collected. Protein concentration were determined using the DeNovix DS-11 Spectrophotometer.

2.5 Plasmid Preparation and Purification

2.5.1 Plasmid Preparation

Transformation was carried out using competent *E. coli* DH5α cells (Invitrogen) (EPA approval number GM009, MU001). Cells were incubated with 0.5 µg of plasmid and incubated on ice for 30 minutes followed by heat shock at 42°C for 45 seconds. Reaction mixtures were placed on ice for a further 2 minutes after which 500 µL of sterile S.O.C medium was added. Transformation mixtures were incubated at 37°C for 1 hour with shaking at 250 rpm. Transformation mixtures were then centrifuged at 5000 rpm and 450 µL of supernatant removed. Cells were resuspended in 50 µL and transferred onto LB agar plates supplemented with 100 µL/mL of ampicillin, after which plates were incubated at 37°C overnight.

2.5.2 Plasmid Purification

After transformation of *E. coli* DH5α, a single colony was picked and inoculated into 5 mL of LB supplemented with ampicillin (100 µg/mL). After five hours of incubation at 37°C with shaking at 250 rpm, 500 µL of starter culture was added to 100 mL of LB supplemented with 100 µg/mL of ampicillin and left to grow overnight at 37°C with constant shaking. Plasmids were then extracted using either the Qiagen Plasmid Midi-Kit, or the GeneJET Plasmid Midiprep Kit (Thermofisher). The concentration of purified plasmid was then determined using DeNovix DS-11 Spectrophotometer at 260 nm.

2.6 Histone Expression and Purification

2.6.1 Histone Expression

Homo sapien core histone proteins were grown in 500 mL of LB broth supplemented with T broth buffer (0.17 M KH_2PO_4, 0.72 M K_2HPO_4), 20% glucose, and 100 µg/mL of ampicillin at 37°C with shaking at 200 rpm until OD_{600} reached 0.4-0.6. Cells were then induced with 0.25 mM of IPTG for 2 hours at 37°C. Pellets were harvested at 5000 rpm for 15 minutes at 4°C and stored at -80°C until purification.

2.6.2 Histone Purification

E. coli BL21 cell pellets were washed with W buffer (50 mM Tris-Cl pH 7.5, 100 mM Nacl, 1 mM 2-mercaptoethanol), after which 50 units of DNase I and 10 mM of $MgCl_2$ was added before the pellet was sonicated at 25% amplitude for 2 seconds on and 8 seconds off for 1 minute. Lysates were then centrifuged at 25K g at 4°C for 20 minutes and combined with WT buffer (W buffer + 1% Triton-X 100 (v/v)). Lysates were then resuspended with 7 M guanidinium HCl solution (7 M guanidinium HCl, 20 mM NaOAc pH 5.2, 1 mM DTT) and left to incubate overnight to unfold histone proteins. After overnight incubation, cell suspensions were centrifuged at 25K g at 4°C for 20 minutes and separated on a Superdex

S-200 ion exchange column (Sigma Aldrich).

Fractions of interest were combined and dialysed with urea buffer (7 M urea, 20 mM NaOAc pH 5.2, 1 mM DTT) overnight. Proteins were then further separated on a disposable column with sequential addition of 10 mL of S100-S1000 buffers in order of increasing salt concentration as in Table 2.1.

Buffer	Composition
S100	7 M Urea 20 mM NaOAc pH 5.2 100 mM NaCl 2 mM BME
S150	7 M Urea 20 mM NaOAc pH 5.2 150 mM NaCl 2 mM BME
S200	7 M Urea 20 mM NaOAc pH 5.2 200 mM NaCl 2 mM BME
S300	7 M Urea 20 mM NaOAc pH 5.2 300 mM NaCl 2 mM BME
S500	7 M Urea 20 mM NaOAc pH 5.2 500 mM NaCl 2 mM BME
S1000	7 M Urea 20 mM NaOAc pH 5.2 1000 mM NaCl 2 mM BME

Table 2.1: Salt Gradient Buffer Compositions. Buffer S100-S1000 were made and 10 mL was added sequentially to the disposable column as in section 2.5.2.

After protein separation, fractions of interest were combined and dialysed in 3 L of water containing 2 mM of BME at 4°C overnight. Samples were centrifuged at 30K g for 20 minutes at 4°C and were then lyophilised.

2.6.3 Histone Octamer Reconstitution

Purified histone proteins were combined in equimolar ratios and rotated at 4°C for 1 hour, after which they were centrifuged at full speed for 30 minutes at 4°C.

Histone octamers were then resolved using a Superdex S-200 column in refolding buffer (7 M guanidinium HCl, 20 mM Tris, pH 7.5, 10 mM DTT). Fractions of interest were combined, concentrated, dialysed in storage buffer (10 mM Tris-Cl, 1 mM EDTA, 2.5 mM NaCl, 25%glycerol, 2 mM BME). Octamer concentration was measured using BSA standards, aliquoted, and stored at -80°C.

2.6.4 SDS-PAGE

For sodium dodecyl sulfate (SDS) poly-acrylamide gel electrophoresis (PAGE), firstly a 12% acrylamide:bis-acrylamide resolving gel was made using 375 mM of Tris-Cl (pH 8.8), 0.1% ammonium persulfate (APS), 0.1% SDS and 0.1% tetramethylethylenediamine (TEMED). A 4% acrylamide:bis-acrylamide stacking gel was made using 125 mM of Tris-Cl (pH 6.8), 0.1% APS, 0.1% SDS and 0.1% TEMED. Once the resolving gel has polymerised, the stacking gel was poured on top and also left to polymerise.

6x SDS-loading buffer (62.5 mM Tris-Cl pH 6.8, 1.67% SDS, 7.5% glycerol, 0.01% bromophenol-blue, 35.75 mM 2-mercaptoethanol) was added to samples at a final concentration of 1x. Samples were heated to 95°C for 5 minutes, after which they were centrifuged and resolved on a 12% acrylamide gel in 1x TGS buffer (25 mM Tris-Cl, 192 mM glycine, 0.1% SDS) at 40 mA for 1 hour.

2.6.5 Coomassie Staining

After resolving samples in a 12% acrylamide gel for 1 hour, gels were washed with distilled H_2O and fixed with 30% methanol and 10% acetic acid. They were then stained with Coomassie blue overnight and destained with distilled H_2O.

2.7 *In Vitro* Nuclesomal Array Assembly

2.7.1 Nucleosome Array Assembly

PD-1 derived peptide (MSGTYLCGAISLAPKAQIKESLR) translationally fused to histone H2B N-terminal tail (pET3 plasmid GenScript) were expressed in *E. coli* BL21 cells. Recombinant and unmodified histones were purified according to section (**2.5.2**). Histones were combined in equimolar ratios and dialysed in refolding buffer (10 mM Tris, 2 M NaCl, 1 mM EDTA, and 1 mM BME). PD-1/H2B octamers and pUC19 plasmid containing 16 repeats of the Widom 601 nucleosome positioning sequence were mixed using different volumes of PD-1/H2B octamer to 1 µg of DNA and dialysed in 1 M NaCl dialysis buffer (10 mM Tris-Cl pH 7.5, 1 mM EDTA, 1 M NaCl, 10 mM 2-mercaptoethanol) for 5-6 hours at 4°C, after which it was dialysed 0.75 M dialysis buffer overnight (10 mM Tris-Cl pH 7.5, 1 mM EDTA, 0.75 M NaCl, 10 mM 2-mercaptoethanol). Assemblies were then dialysed in PBS overnight twice at 4°C, after which they were collected and stored at 4°C.

2.7.2 Micrococcal Nuclease Digestion of Nucleosomal Arrays

For each nucleosomal assembly made, an micrococcal nuclease (MNase) digestion was performed. From each assembly, 1 µg of nucleosomal array was made up to 200 µL with PBS, after which 1 µL of 250 mM $CaCl_2$ was added. This was then split into two tubes of 100 µL and incubated at 30°C for 10 minutes. To these tubes, 0.5 µL or 2 µL of MNase (Roche) diluted 1:2000 in salt dilution buffer II (10 mM Tris pH 7.5, 1mM EDTA, 0.1% v/v NP-40, 5mM DTT, 0.5 mM PMSF, 20% v/v glycerol, 100 µg/mL BSA) was added and incubated for a further 10 minutes at 30°C. After incubation, digestion was stopped by adding 300 µL of glycogen stop buffer (20 mM EDTA, 0.2M NaCl, 1% v/v SDS, and 0.25 mg/mL glycogen), 1 µL of 50 mg/mL Proteinase K, and 16 µL of 250 mM EGTA to each reaction. This was incubated overnight at 37°C, after which 25 µL of 5 M NH_4AC was added, and DNA was extracted using 1:1 phenol and chloroform.

DNA was then ethanol precipitated and centrifuged at max speed for 15 mins at 4°C. Pellets were resuspended in TE buffer (10 mM Tris-Cl, 1 mM EDTA) and electrophoresed on 1.2% agarose gel. DNA bands were visualised using ethidium bromide (EtBr) and imaged with a UV transilluminator.

2.8 Microscopy Techniques

2.8.1 Acid etching and Poly-D-lysine Coverslip Coating

Coverslips (Electron Microscopy Sciences 8 mm Diameter, #1.5 Thickness) were first incubated in 1M HCl overnight at 60°C in a covered beaker. The next day, they were washed with sterile dH2O to remove excess acid. Coverslips were then incubated with 1 mg/mL of poly-D-lysine (Sigma-Aldrich) for 1 hour at room temperature on a shaker. Coverslips were washed 3 x with sterilised dH_2O, 2 x 10 minutes 70% EtOH, and lastly 2 x 10 minutes with 100% EtOH. After drying on filter paper, coverslips were UV treated in a laminar flow hood for 20 minutes on each side, after which they were stored at 4°C with minimal disruption.

2.8.2 Immunofluorescence

U87-MG and MCF-7 were seeded on top of poly-D-lysine coated coverslips in a 6-well plate at a density of 2.5 x 10^5 cells/well and left overnight to grow. Cells were washed 2 x for 3 minutes PBS (+MgCl) at room temperature, and subsequently fixed with 4% paraformaldehyde (in PBS) for 15 minutes and washed 2 x 10 minutes with PBS. Cells were then permeabilised using 2 mL of 1x PBS containing 0.5% Triton-X for 5 minutes and washed again with PBS. After transferring coverslips to a 24-well plate, they were incubated with blocking buffer (10% BSA, 0.5% Tween-20, 1x PBS) for 30 minutes. Cells were washed 2 x 3 minutes in PBS, after which they were incubated overnight at 4°C with primary antibody (Dako Anti-PD-L1 antibody [28-8], Abcam) diluted 1:350 to 2.85 µg/µL in blocking buffer. After overnight incubation, excess primary antibody was removed and cells were washed 3 x 5 minutes with wash buffer (1x PBS, 0.1% Triton-X) and

incubated with secondary antibody diluted 1:500 in blocking buffer (Goat Anti-Rabbit IgG H&L Alexa Fluor® 555, Abcam) for 1 hour at room temperature. Cells were then washed 3 x 5 minutes in wash buffer and 1 x 5 minutes in PBS, and were then fixed with 2% paraformaldehyde for 15 minutes. After washing 2 x 5 minutes with PBS, the coverslips were then mounted using SlowFade® Gold Antifade Mountant with or without DAPI counterstain.

2.8.3 Fluorescent Labelling of PD-1/H2B Nucleosomal Arrays

U87-MG and MCF-7 cells were seeded on top of poly-D-lysine coated coverslips in a 6-well plate at a density of 2.5 x 10^5 cells/well and left overnight to grow. Cells were washed 2 x for 3 minutes PBS (+MgCl) at room temperature, and subsequently fixed with 4% paraformaldehyde (in PBS) for 15 minutes and washed 2 x 10 minutes with PBS. If permeabilisation was required, cells were permeabilised using 2 mL of 1x PBS containing 0.5% Triton-X for 5 minutes and washed again with PBS. After transferring coverslips to a 24-well plate, they were incubated with blocking buffer (10% BSA, 0.5% Tween-20, 1x PBS) for 30 minutes. If herring sperm DNA was used, it was at this step and diluted to 100 µg/mL in blocking buffer. Before application to cells, 1 µg of nucleosomal array was preincubated with 2 µg/ml of NeutriAvidin™ Oregon Green™ 488 conjugate (Thermofisher) for 2 hours at room temperature. Cells were washed 2 x 3 minutes in PBS and subsequently 3 x 5 minutes in wash buffer, after which they were incubated with 1 µg of array-Avidin-488 conjugate for 1 hour. Excess nucleosomal array was removed, and cells were washed 3 x 5 minutes with wash buffer and 1 x 5 minutes in PBS. Stained cells were then fixed with 4% paraformaldehyde (in PBS) for 15 minutes and washed 2 x 5 minutes with PBS. If cells were unpermeabilised, they were firstly counterstained with Hoescht 3342 to image the nuclear DNA, and mounted using SlowFade® Gold Antifade Mountant without DAPI. Permeabilised cells were mounted with SlowFade® Gold Antifade Mountant containing DAPI.

2.9 Alternative Detection Methods

2.9.1 Fluorescence Capture Through Roche 480 Lightcycler Software

U87-MG cells were grown to 80-90% confluency, after which they were harvested and diluted to 5 x 10^6 cells/mL. Cells were centrifuged at 220g for 5 minutes and resuspended in PBS, after which 100 µL of cells were incubated with either 0, 0.1 µg, 0.5 µg, 1 µg, 2 µg, or 5 µg of PD-1/H2B-Cy5 nucleosomal array or wild-type-Cy5 nucleosomal array. Cells were incubated at room temperature in the dark for 2 hours, after which cells were washed with PBS and centrifuged at 380g for 5 minutes. Cells were resuspended in a final volume of 50 µL and fluorescence was captured using the Roche 480 Lightcycler. The Cy5 filter (615-670 nm) was used as the Cy5 fluorophore excites at 649 nm and emits at 666 nm. The program was set as follows: 1 cycle at 95°C with a 5 minute hold followed by 12 cycles at 37°C with a 5 second hold. Fluorescence readings were only taken during the 12 cycle period.

2.9.2 Fluorescence Activated Cell Sorting (FACS)

U87-MG and MCF-7 cells were grown to 80-90% confluency, harvested, and resuspended at a density of 5 x 10^5 cells/mL. Cells were centrifuged at 220g for 5 minutes and resuspended in PBS, after which 100 µL of cells were incubated with either with 0.1 µg, 0.5 µg or 1 µg of PD-1/H2B-Cy3 nucleosomal arrays for 2 hours in the dark at room temperature, after which cells were centrifuged at 380g for 5 minutes, fixed using 4% paraformaldehyde, and washed once more. Cells were resuspended in a final volume of 1 mL before cell populations were separated using the MoFlo XDP Cell Sorter at a flow rate of 50 µL/min. The R-phycoerythrin (PE) filter (Ex 566 nm Em 574) was used to detect the Cy3 fluorophore and the fluorescein (FITC) filter (Ex 490 nm, Em 525 nm) was used to detect any fluoresence emitted at a smaller wavelength.

Chapter 3

Creation and Optimization of the PD-1/H2B Nucleosomal Arrays

3.1 Histone Expression and Purification

To create the PD-1 tagged H2B nucleosomal arrays required the expression of PD-1/H2B and the other core histones, labelling of the nucleosomal positioning DNA and formation of nucleosomal arrays. To obtain purified chimeric PD-1/H2B histone, initially the PD-1/H2B expression vector was created by cloning the PD-1 cDNA fragment (amino acid 118-139) in front of the H2B sequence in a pET3a vector. This was done by Dr. Jeong Park. Histone H2B was chosen as it is located on the surface of the histone octamer dimerised with histone H2A, as opposed to either histones H3 or H4 which form the histone octamer core (Arents et al., 1991). The amino acid sequence and schematic diagram of the chimeric PD-1/H2B is shown in Figure 3.1.

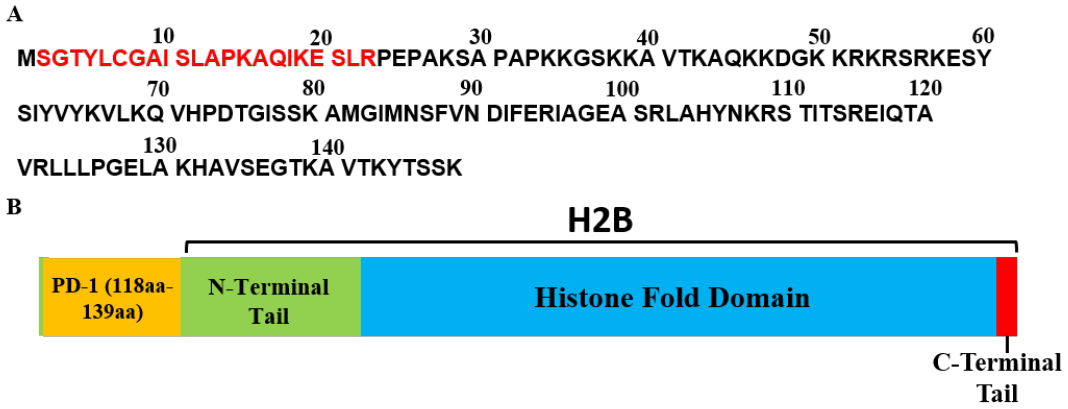

Figure 3.1: Chimeric Histone H2B Sequence and Structure. **A**, Amino acid sequence of histone H2B with PD-1 amino acids 118-139 insertion indicated in red. PD-1 peptide was inserted after the first amino acid, M, of histone H2B. **B**, schematic diagram of chimeric histone H2B.

Histones were then expressed and purified so histone octamers containing H2A, PD-1/H2B, H3, and H4 could be formed. This was done according to previously established methods (Kintsler et al., 2019) (see Section **2.5**). The following figures are from the expression and purification of histone H4 as histones H2A, PD-1/H2B, and H3 were previously purified by Dr. Jeong Park. H4 histone plasmid vector (pET3a-H4) was obtained from Genecript and expressed in *E. coli* DH5α cells. *E. coli* cells were transformed with pET3-H4 plasmid, expressed and induced with IPTG, and proteins were resolved using SDS-PAGE (Figure 3.2).

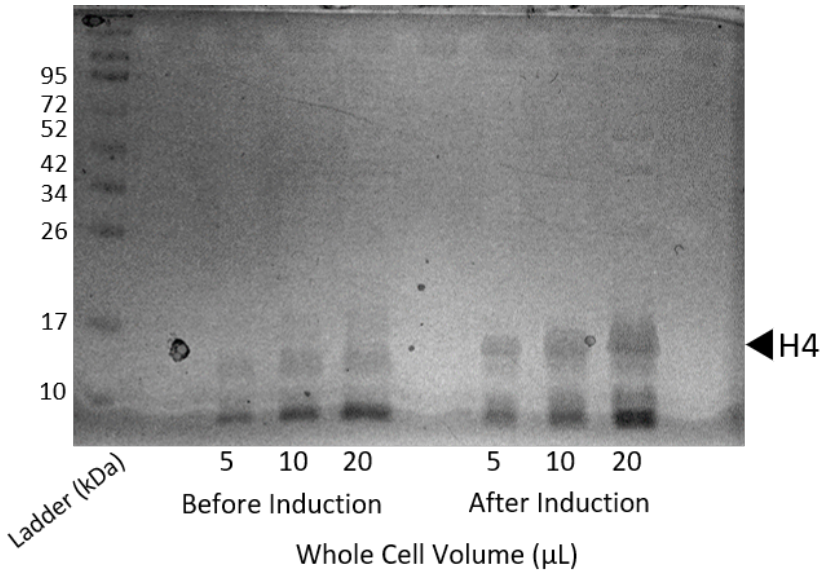

Figure 3.2: Induction of H4 Expression. *E. coli* was transformed with H4 expression vector (pET3a-H4) and induced with 0.25 mM of IPTG for 2 hours after which it was harvested. Samples of whole cell before and after induction was resolved on a 12% SDS-PAGE and stained with Coomassie blue (see Section **2.5.4** and **2.5.5**). The expected molecular weight of histone H4 is approximately 11 kDa.

After induction of H4 expression, the bands which ran at approximately 12 kDa are darker indicating that histone H4 had been expressed. Cells were then sonicated and centrifuged to collect soluble (supernatant) and insoluble (pellet) fractions. After resolution on a 12% SDS-PAGE, this indicated that H4 was present in the cell pellet and whole sonicate as only these two lanes have visible bands (Figure 3.3).

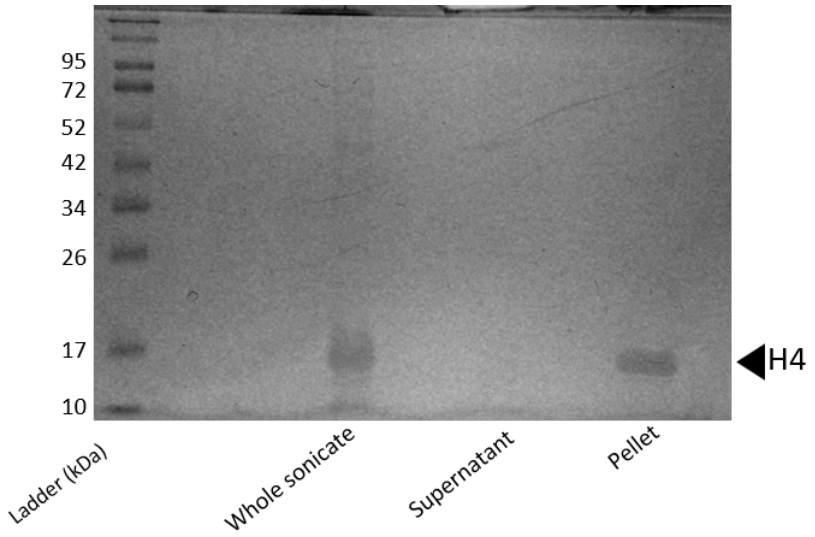

Figure 3.3: Histone H4 is Found in the Pellet. After harvesting, cell pellets were resuspended in W buffer and sonicated at 25% amplitude for 1 minute. Samples were centrifuged and 10 µL of sample was resolved on a 12% SDS-PAGE and stained with Coomassie blue. Protein ladder was run adjacent to samples.

Histones were then denatured using guanidinium hydrochloride after which ion exchange chromatography was performed using a SP Sepharose s200 column (see Section **2.5.2**).

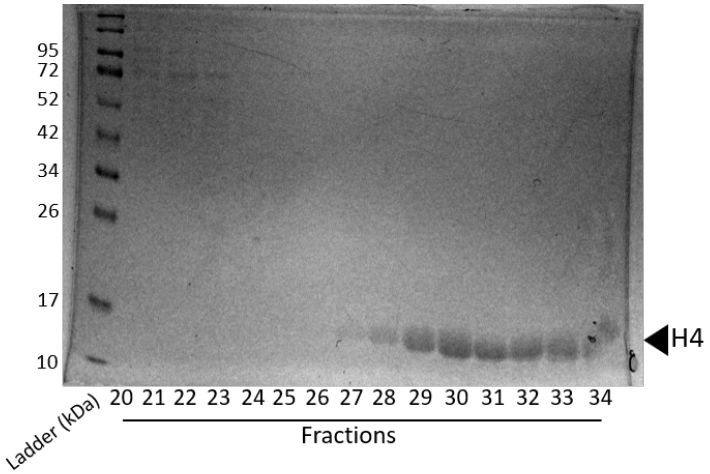

Figure 3.4: S-200 Superdex H4 Histone Fractions. After histone inclusion bodies were separated and histones unfolded using guanidinium hydrochloride, the histone H4 sample was applied to a S-200 Superdex column and resolved at 0.2 mL/min in 3 mL fractions. Fractions were separated on using a 12% SDS-PAGE and stained with Coomassie blue. Protein ladder was run adjacent to samples.

Fractions of interest (29-34) were combined (Figure 3.4), dialysed in urea buffer and passed over a disposable ion exchange column using six different salt buffers applied in order of increasing salt concentration. Composition of these buffers is detailed in **Table 1.1** in Section **2.5.2**. Once this had been completed, histone fractions were dialysed in urea buffer and lyophilised for storage.

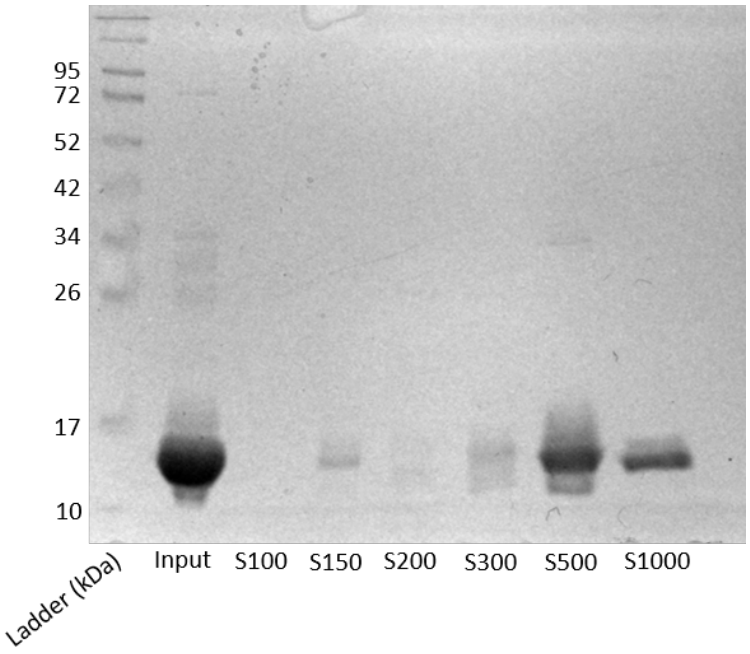

Figure 3.5: Ion Exchange H4 Elutions. H4 samples were applied to an ion exchange column and subjected to different salt gradient buffers to elute histone H4. From each elution, 10 µL was taken and resolved on a 12% SDS-PAGE and stained with Coomassie blue. Protein ladder was run adjacent to samples.

After purifying H4 with ion exchange chromatography, purity was then checked by resolving different amounts of histone H4 on a 12% SDS-PAGE, alongside previously purified histone H3 (Figure 3.6). One band was seen in each of the histone H4 lane indicating that it has been purified.

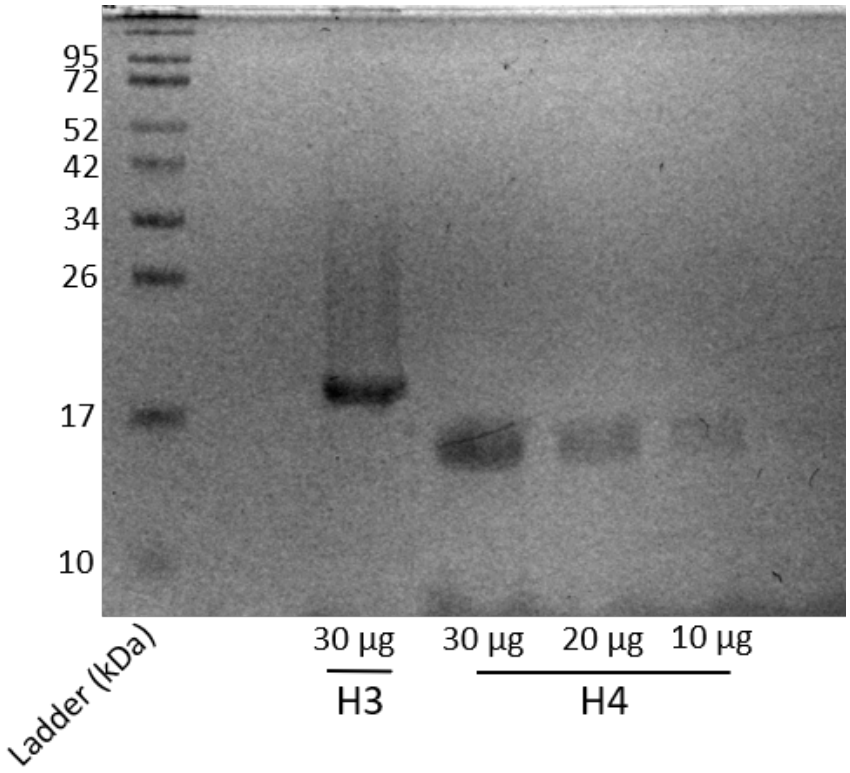

Figure 3.6: Purified Histone H4. To check for histone purity, 10, 20, and 30 µg of histone H4, and 30 µg of histone H3 were resolved on a 12% SDS-PAGE and stained with Coomassie blue. Protein ladder was run adjacent to samples. The expected molecular weights of histones H4 and H3 are 11 kDa and 15 kDa respectively.

To begin histone octamer reconstitution, each purified histone was first dialysed in unfolding buffer (see Section **2.5.3**). Histones H2A and H2B were then mixed in equimolar ratios to form dimers, as were histones H2B and PD-1/H2B. The same process was done with histones H3 and H4 to form tetramers (Figure 3.7). The full gel image of Figure 3.7 is shown in Figure A.1.

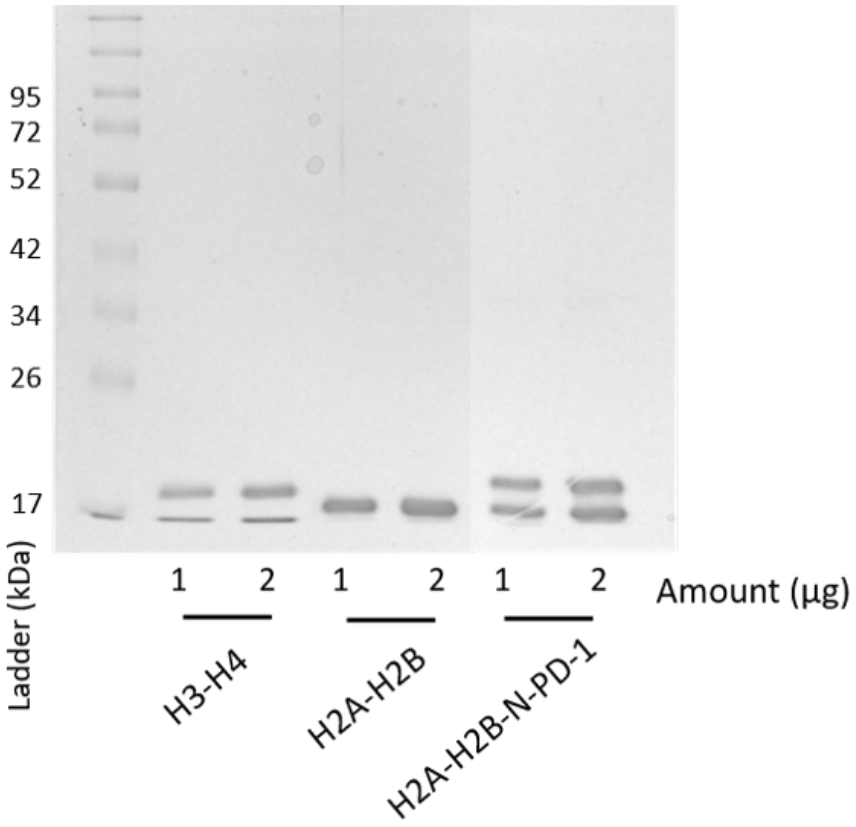

Figure 3.7: Purified H2A-H2B Dimers and H3-H4 Tetramers. Histone proteins were mixed in equimolar ratios to make the indicated dimers and tetramers. All samples were diluted to 40 mM and 1 or 2 µg were resolved on a 12% SDS-PAGE and stained with Coomassie blue. Protein ladder was run adjacent to samples. H2A-H2B-N-PD-1, PD-1 ligand peptide attached to the N-terminal of H2B. The expected molecular weights of histones H4, H3, H2A, and H2B are 11 kDa, 15 kDa, 14 kDa, and 14 kDa for each histone respectively. Lanes not relevant to this study have been removed during image processing. The full gel image of Figure 3.9 is shown in Figure A.1.

After the H2A PD-1/H2B dimers and H3-H4 tetramers were combined to form octamers, they were then dialysed in refolding buffer, centrifuged, and concentrated. PD-1/H2B histone octamers were then purified on a Superdex-200 column and the histone octamers eluted, after which their concentration was measured using the DeNovix DS-11. Fractions of interest (22-35) were then pooled, concentrated, then dialysed in final dialysis buffer (Figure 3.8) (see Section **2.5.3**).

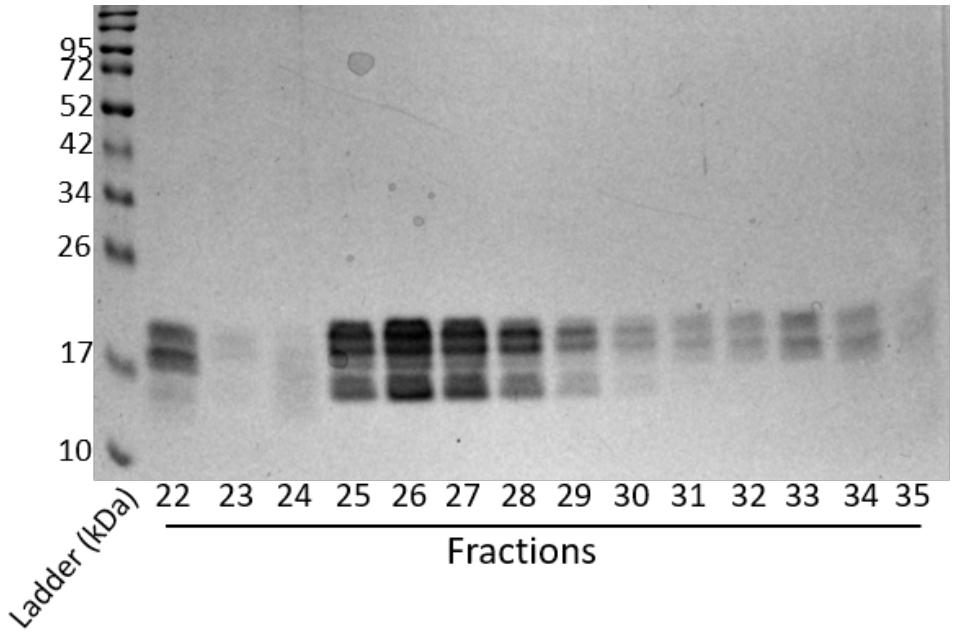

Figure 3.8: PD-1/H2B Histone Octamer Fractions. After mixing H2A-H2B-N-PDR dimers and H3-H4 tetramers in equimolar ratios, samples were purified using a S-200 Superdex column at 0.1 mL/min at 1 mL fractions. From each fraction, 10 µL was taken and resolved on a 12% SDS-PAGE and stained with Coomassie blue. Protein ladder was run adjacent to samples. The expected molecular weights of histones H4, H3, H2A, and H2B are 11 kDa, 15 kDa, 14 kDa, and 14 kDa for each histone respectively.

Purified PD-1/H2B histone octamers were resolved on a 12% SDS-PAGE. In Figure 3.9, four bands can be seen when using the highest sample amount of PD-1/H2B histone octamers. The four bands represent the four histone proteins used to form the octamers. These four bands run from approximately 15 kDa to 21 kDa. WT octamers that contain untagged histone H2B were formed previously by Dr. Jeong Park.

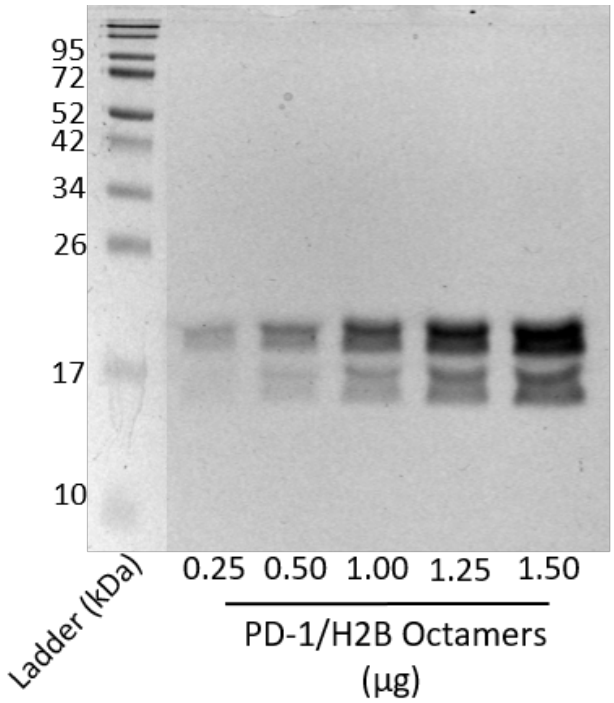

Figure 3.9: Purified PD-1/H2B Histone Octamers. After PD-1/H2B histone octamers were purified, 0.25, 0.5, 1.00, 1.25, and 1.50 µg of PD-1/H2B octamer was separated using 12% SDS-PAGE and stained with Coomassie blue. Protein ladder was run adjacent to samples. The expected molecular weights of histones H4, H3, H2A, and H2B are 11 kDa, 15 kDa, 14 kDa, and 14 kDa for each histone respectively. Lanes not relevant to this study have been removed. The full gel image of Figure 3.9 is shown in Figure A.2.

3.2 Formation of the PD-1/H2B Nucleosomal Arrays

To determine the optimal ratio of DNA to histone octamers, nucleosomal assembly titrations were performed then analysed by Micrococcal nuclease (MNase) digestion to confirm phased nucleosomes. MNase is an endonuclease that digests DNA non-specifically between the linker regions of histones (Heins et al., 1967). This produces a ladder of descending single, double, and poly-nucleosomes if nucleosomes are properly positioned.

Nucleosomal arrays were assembled using 1 µg of pUC19 DNA containing 16 repeats of the Widom 601 nucleosome positioning sequence and increasing amounts of PD-1-H2B histone octamers ranging from 0.25 µg to 1.25 µg. Two different concentrations of MNase were used to ensure partial digestion of the arrays.

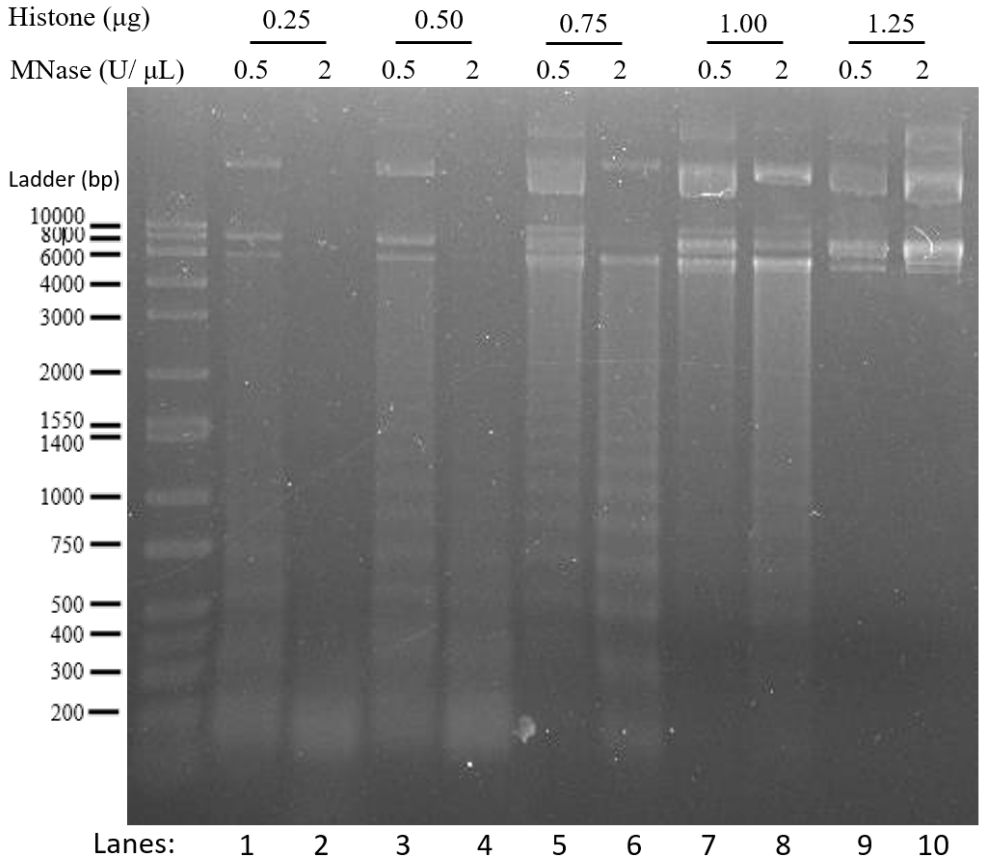

Figure 3.10: Micrococcal Nuclease Digestion of Assembled Nucleosomal Arrays. Nucleosomal arrays were made using 1µg/µL of un-labelled pUC19 plasmid DNA containing 16 repeats of the Widom 601 nucleosome positioning sequence and increasing amounts of PD-1-H2B histone octamers. After mixing, arrays were dialysed in decreasing salt gradient buffers and digested with 0.5 and 2 U/µL of MNase. DNA fragments were resolved on a 1.2% agarose gel and stained with ethidium bromide. DNA ladder was run adjacent to the samples.

As seen in Figure 3.10, using 0.75 µg of histone octamer to 1 µg of DNA creates the most discernible DNA ladder which reflects properly spaced nucleosomes (lanes 5 and 6) and gives a similar ladder to a nucleosomal array with untagged histone (Voong et al., 2017). A lower amount of histone octamer (0.25 µg) results in little discernible ladder indicating this concentration of core histones results in

an array undersaturated with nucleosomes as the nucleosomes are too distantly spaced resulting in indiscriminate cleavage by MNase (lanes 1 and 2). In lanes 9 and 10, no ladder can be seen when using a histone octamer amount of 1.25 µg, indicating the array is over-saturated with histones. Therefore nucleosomal arrays containing 0.75 µg of PD-1-H2B histone octamers per 1 µg of nucleosomal positioning plasmid DNA were used for the remainder of this study in order to obtain uniform nucleosome spacing.

3.3 Fluorescently Labelling Nucleosomal Array DNA

In order to detect the PD-1/H2B nucleosomal array, it was necessary to fluorescently label the DNA which contains 16 repeats of the Widom 601 nucleosome assembly sequence. DNA was labelled using the Mirus *Label* IT® Nucleic Acid Labelling Kit, Cy®3. This was performed by Dr. Jeong Park. Fluorescent labelling was selected as it is efficient and can be quantified directly and easily. Fluorophores are able to attach to multiple sites on the nucleosomal array DNA which ensures amplification of signal.

After determining the optimal ratio of histone octamers to DNA, it was then necessary to compare PD-1-H2B nucleosomal assemblies made with both Cy3 labelled DNA and unlabelled DNA to determine whether the fluorophore labelling affected nucleosome positioning, or causes DNA to aggregate such that the arrays can no longer be cleaved by MNase. For this experiment, 0.75 µg of octamers were mixed with 1 µg of unlabelled DNA as this was the optimal ratio determined from Figure 3.10. This was compared to nucleosomal arrays assembled with different amounts of PD-1/H2B octamers and 1 µg of Cy3-labelled DNA. All assemblies were MNase digested, DNA isolated and fragments were resolved on a 1.2% agarose gel.

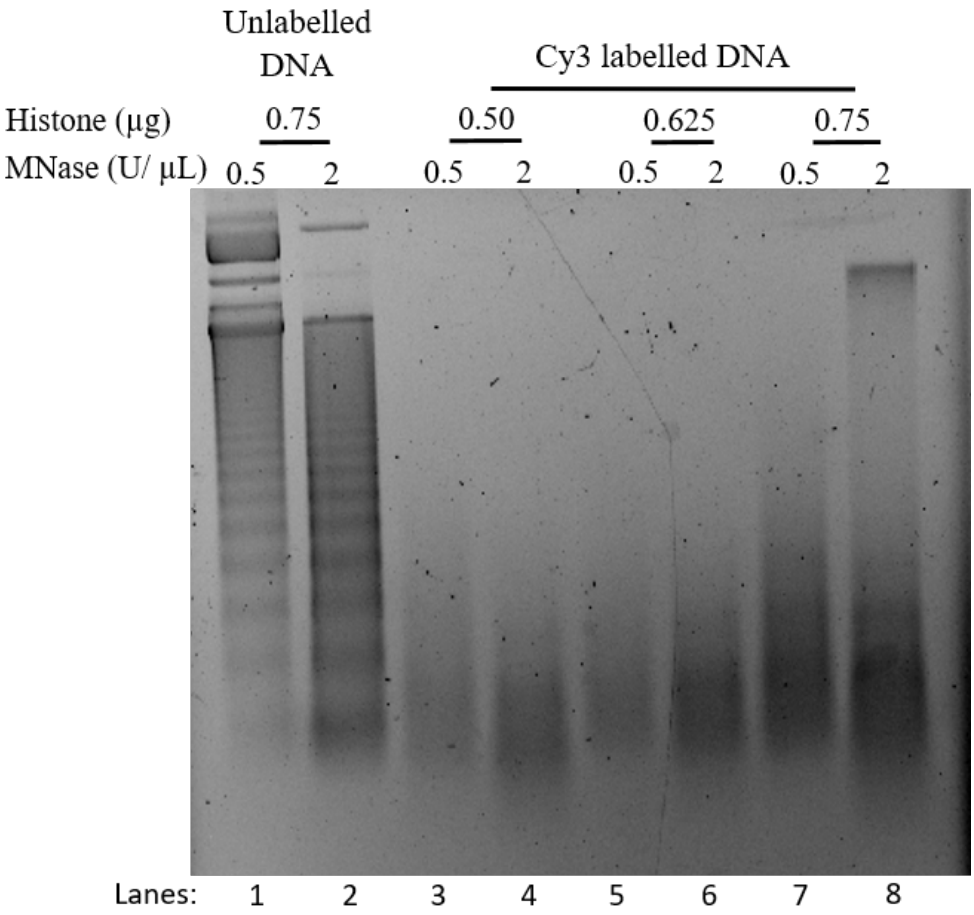

Figure 3.11: Micrococcal Nuclease Digestion of Unlabelled and Cy3 Labelled Nucleosomal Arrays. MNase assay of nucleosomal arrays using 1µg/µL of unlabelled pUC19 plasmid DNA and Cy3 labelled pUC19 plasmid DNA containing 16 repeats of the Widom 601 nucleosome positioning sequence, and increasing amounts of PD-1-H2B histone octamers as indicated. After mixing, assemblies were digested with 0.5 and 2 U/µL of MNase. DNA fragments were resolved on a 1.2% agarose gel and stained with ethidium bromide. DNA ladder was run adjacent to the samples.

As seen in Figure 3.10, an array assembled using unlabelled DNA with PD-1-H2B histone octamers resulted in a distinctly spaced DNA ladder, indicating appropriate nucleosome spacing. When comparing this to nucleosomal arrays assembled using Cy3 labelled DNA, however, there were indications that Cy3 affects nucleosomal array formation. MNase digestion of nucleosomal arrays made with unlabelled DNA (lanes 1 and 2) show the distinctive ladder as seen in lanes 5 and 6 in Figure 3.10. The lack of distinct bands in lanes 3-8 (Figure 3.11) is comparable to previous assemblies made with 0.25 µg of the PD-1/H2B histone

octamers (Figure 3.10 lanes 1 and 2) which are under-saturated with histones. Very faint bands can be seen in lanes 7 and 8 (Figure 3.11), but the lack of distinct bands suggests that this assembly does not have correctly phased nucleosomes. This suggests that the Cy3 label affects nucleosomal array formation.

Labelling DNA with a Cy3 fluorophore and forming nucleosomal arrays using lower amounts of PD-1/H2B octamers does not form correctly phased nucleosomes (Figure 3.11) as using 0.75 µg of PD-1/H2B octamers did not result in a discernible ladder. Next, it was questioned whether this type of fluorescent labelling required higher amounts of histone octamers for the DNA backbone to be saturated with nucleosomes. Nucleosomal arrays were assembled using 0.75 µg to 1.50 µg of PD-1/H2B histone octamers and Cy3 labelled DNA. Arrays were made using salt gradient buffer dialysis, and were digested with MNase. Detection of the DNA ladder was achieved by exciting the Cy3 fluorophore instead of staining agarose gels with ethidium bromide to confirm the ability to detect fluorescent nucleosomal arrays.

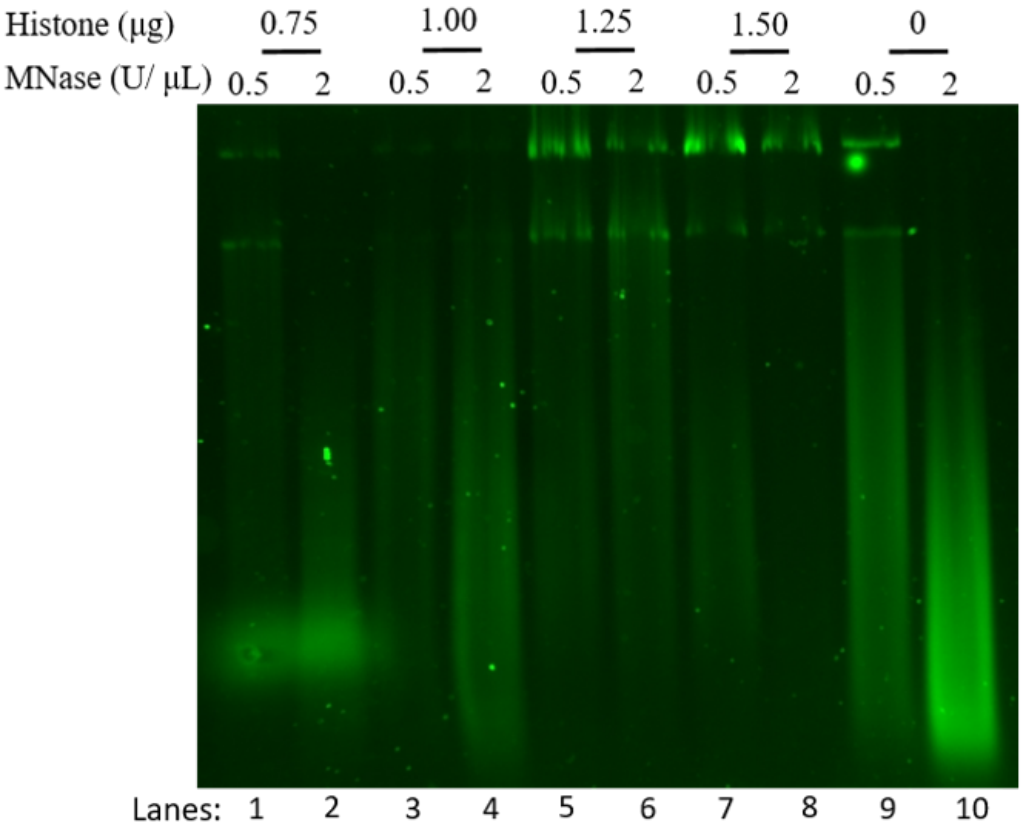

Figure 3.12: Micrococcal Nuclease Digestion of Cy3 Assemblies and Cy3 Labelled DNA. MNase assay of nucleosomal arrays using 1µg of Cy3 labelled pUC19 plasmid DNA and increasing amounts of PD-1-H2B histone octamers as indicated, or 1 µg of Cy3-labelled pUC19 DNA alone (0 µg). Assemblies were digested with 0.5 and 2 U/µL of MNase. DNA fragments were resolved on a 1.2% agarose gel. Fluorescence images were captured on the Azure c600 software using the Cy3 channel (Ex: 554 nm, Em: 568 nm).

From Figure 3.12, using 0.75 µg (lanes 1 and 2) of PD-1/H2B octamers did not result in a discernible ladder, unlike the digests in Figure 3.10 using the same amount of histone octamer. This is also the case when assemblies are made with 1 µg of PD-1/H2B octamers. The smearing of the DNA ladder in all assembly lanes appear similar, though with much less intensity, to DNA alone (lanes 9 and 10). This indicates that the assemblies were likely under-saturated with histones as using either concentration of MNase gives the same smear. When higher amounts of histone octamers were used however, not only is there no discernible ladder, but there is also DNA aggregation in the wells regardless of whether a

higher concentration of MNase was used (lanes 5-8). This is likely caused by the increased histone amount (1.25 µg and 1.50 µg). There is also DNA aggregation in the DNA only (0 µg of PD-1/H2B) lanes 9 and 10. This may also indicate that the PD-1 tag on the N-terminal of histone H2B could be affecting nucleosome formation.

To investigate whether the H2B tagged with PD-1 affects the formation of nucleosomes, assemblies were made using 1 µg of Cy5-labelled nucleosome positioning DNA and 0.75 µg of WT histone octamers. Assemblies were dialysed in decreasing salt buffers and digested with MNase as in previous experiments. DNA fragments were resolved on a 1.2% agarose gel and the fluorescence image captured using Azure c600 software using the Cy3 channel.

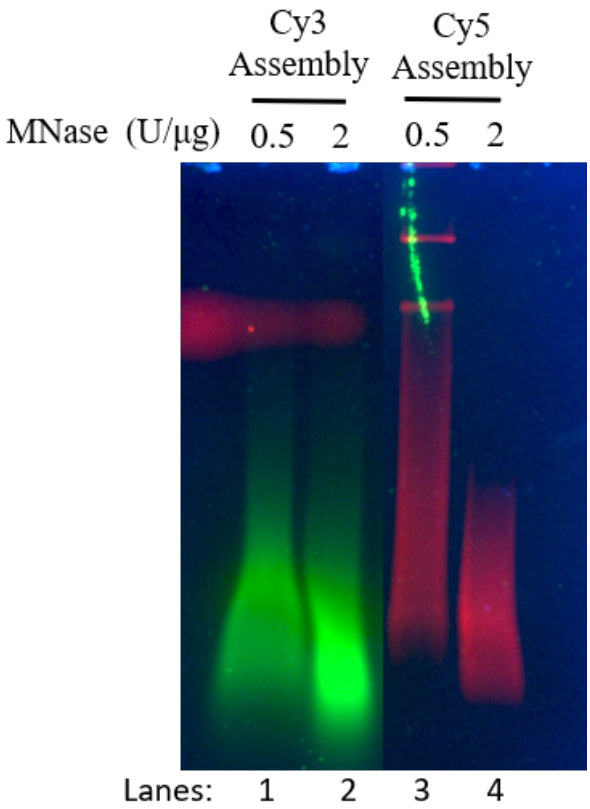

Figure 3.13: Micrococcal Nuclease Digestion of Cy3 and Cy5 Nucleosomal Arrays. MNase assay of nucleosomal arrays using 1µg of Cy3 or Cy5 labelled pUC19 plasmid DNA containing 16 repeats of the Widom 601 nucleosome positioning sequence and 0.75 µg WT octamers. Assemblies were digested with 0.5 and 2 U/µL of MNase. DNA fragments were resolved on a 1.2% agarose gel. Fluorescence images were captured on the Azure c600 software using the Cy3 and Cy5 channels.

Figure 3.13 shows that nucleosomal arrays made using 0.75 µg of PD-1/H2B histone octamers and either Cy3 or Cy5 labelled DNA results in a smear of DNA, indicating that nucleosomes are not correctly phased, if formed at all. This is similar to Figure 3.12 when using 0.75 µg of PD-1/H2B histones. These findings demonstrate that nucleosomal arrays made with either Cy3 or Cy5 labelled DNA did not form properly positioned nucleosomal arrays. Due to this inconsistency, a non-fluorophore label was tested in order to detect DNA.

Given the above issues, the pUC19 plasmid containing 16 Widom sequence repeats was biotin labelled, then bound with Avidin-Alexa 488 to enable fluorescence detection. Biotin labelling was performed using the EZ-Link® Psoralen-PEG_3-Biotin kit. A nucleosomal array was assembled using 5 µg of biotin-labelled pUC19 plasmid and 3.75 µg of PD-1/H2B octamers as per Section **2.6.1**. To confirm nucleosomal array formation, a MNase assay was performed and visualised. As seen in Figure 3.14, there is a distinct DNA ladder when using a lower concentration of MNase indicating appropriate nucleosomal array formation.

Nucleosomal arrays formed with PD-1/H2B octamers and biotin-labelled DNA formed correctly spaced nucleosomes and this array was used to test binding to PD-L1 on the surface of cells. To determine if nucleosomal arrays had the distinct "beads on a string" structure (Olins and Olins, 1974), they were visualised by transmission electron microscopy (TEM). PD-1/H2B-biotin and WT-biotin nucleosomal arrays were formed using the salt buffer dialysis method (as per Section **2.6.1**) and then stained with 2% uranyl acetate and 1% phosphotungstic acid.

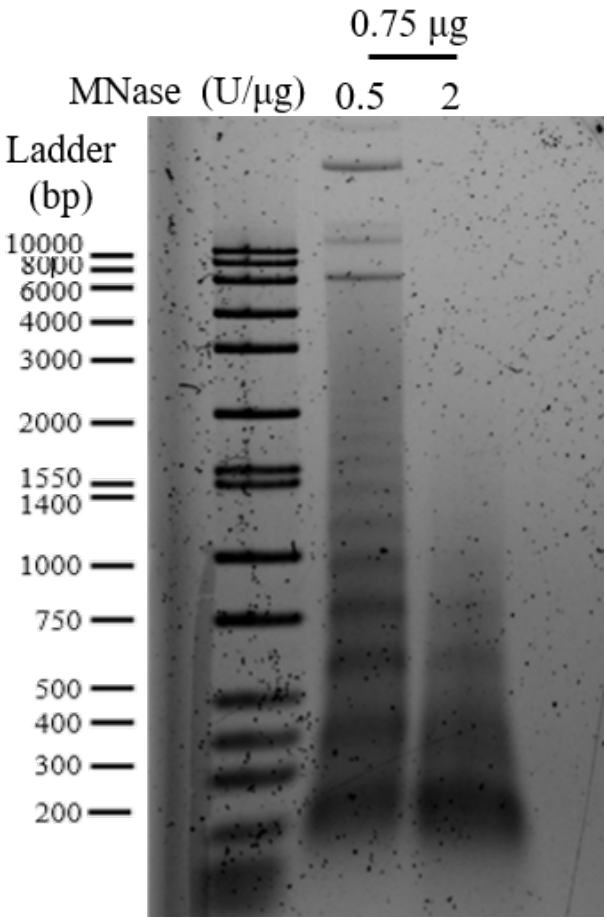

Figure 3.14: Micrococcal Nuclease Digestion of Biotin-Labelled Nucleosomal Arrays. MNase assay of a nucleosomal array made using 1µg/µL of biotin-labelled pUC19 plasmid DNA containing 16 repeats of the Widom 601 nucleosome positioning sequence and 0.75 µg of PD-1-H2B histone octamers. The assembly was digested with 0.5 and 2 U/µL of MNase. DNA was ethanol precipitated, after which they were resolved on a 1.2% agarose gel and stained with ethidium bromide.

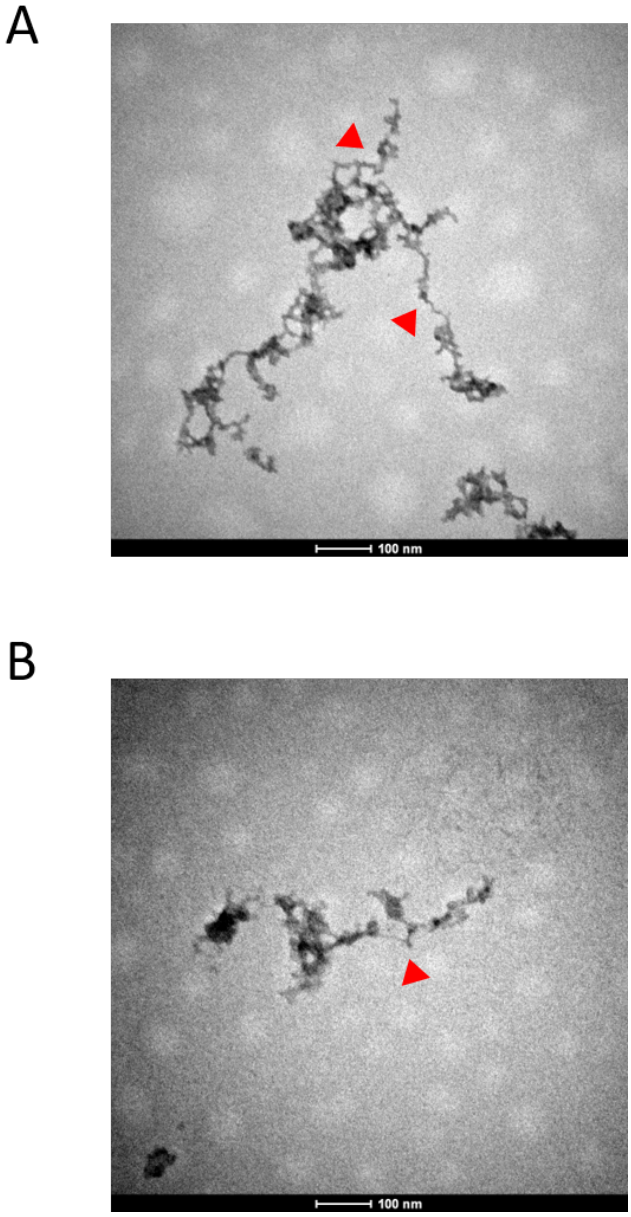

Figure 3.15: TEM Images of WT and PD-1-H2B Assemblies. TEM images of WT and PD-1-H2B assembled nucleosomal arrays using 5µg of biotin-labelled pUC19 plasmid DNA and 3.75 µg of WT (**A**) or PD-1-H2B histone octamers (**B**) diluted to 0.2 ng/µL. Assemblies were then incubated on a carbon-coated graphite grid and stained with 2% uranyl acetate for 5 minutes followed by staining with 1% phosphotungstic acid. Samples were then imaged using FEI Tecnai G2 Spirit BioTWIN transmission electron- microscope. Scale bar: 100 nm

Unfortunately, Figure 3.15 shows both WT and PD-1/H2B nucleosomal arrays do not exhibit the "beads on a string" structure (Baldi et al., 2020). Instead

the arrays aggregate and this is likely due to preparation of the samples. Both Figure 3.15A and Figure 3.15B show some distinct punctate spots indicated by red arrows in both images, however it does not demonstrate an array structure was formed. As WT and PD-1/H2B nucleosomal arrays both look similar, it can be assumed that the PD-1 tag on the N-terminal tail of histone H2B is not the cause of the aggregation. There are ways to overcome aggregation issues when preparing nucleosomal arrays for TEM such as sonication of samples before they are imaged, or dialysing samples over a longer period of time in a different salt buffer (Guo and Cole, 1989).

Chapter 4

Testing of PD-1 Nucleosomal Array to Detect PD-L1 on the Cell Surface

4.1 Selection of Cell Lines

To test the efficacy of PD-1/H2B nucleosomal array binding to PD-L1 on the cell surface, two mammalian cell lines with low and high PD-L1 expression were used to determine if there was differential binding of the PD-1/H2B nucleosomal array. Initially, the Protein Atlas database (The Human Protein Atlas, 2021) was screened to identify potential cell lines for this study. Figure 4.1A indicates the highest PD-L1 protein levels are in glioma cell lines U138-MG, U251-MG, and U87-MG. Amongst the lowest expressing cell lines are sourced from pancreatic cancer cells, kidney and bladder cancer cells, MCF-7 breast cancer cells and Hela cervical cancer cells. In order to confirm results from Protein Atlas, RT-qPCR was performed (see Section **2.2**) on a selection of cell lines (Figure 4.1B). U87-MG had the highest PD-L1 mRNA expression levels followed by LN18. Cell lines H1299, U2OS, and HeLa were also tested and showed moderate to low expression, with MCF-7 showing the lowest mRNA expression level. This is in concordance with in Figure 4.1A. Because MCF-7 and U87-MG cells showed the lowest and highest PD-L1 expression respectively, these cell lines were chosen to test nucleosomal array binding, and compare this binding to that of a diagnostic PD-L1 antibody.

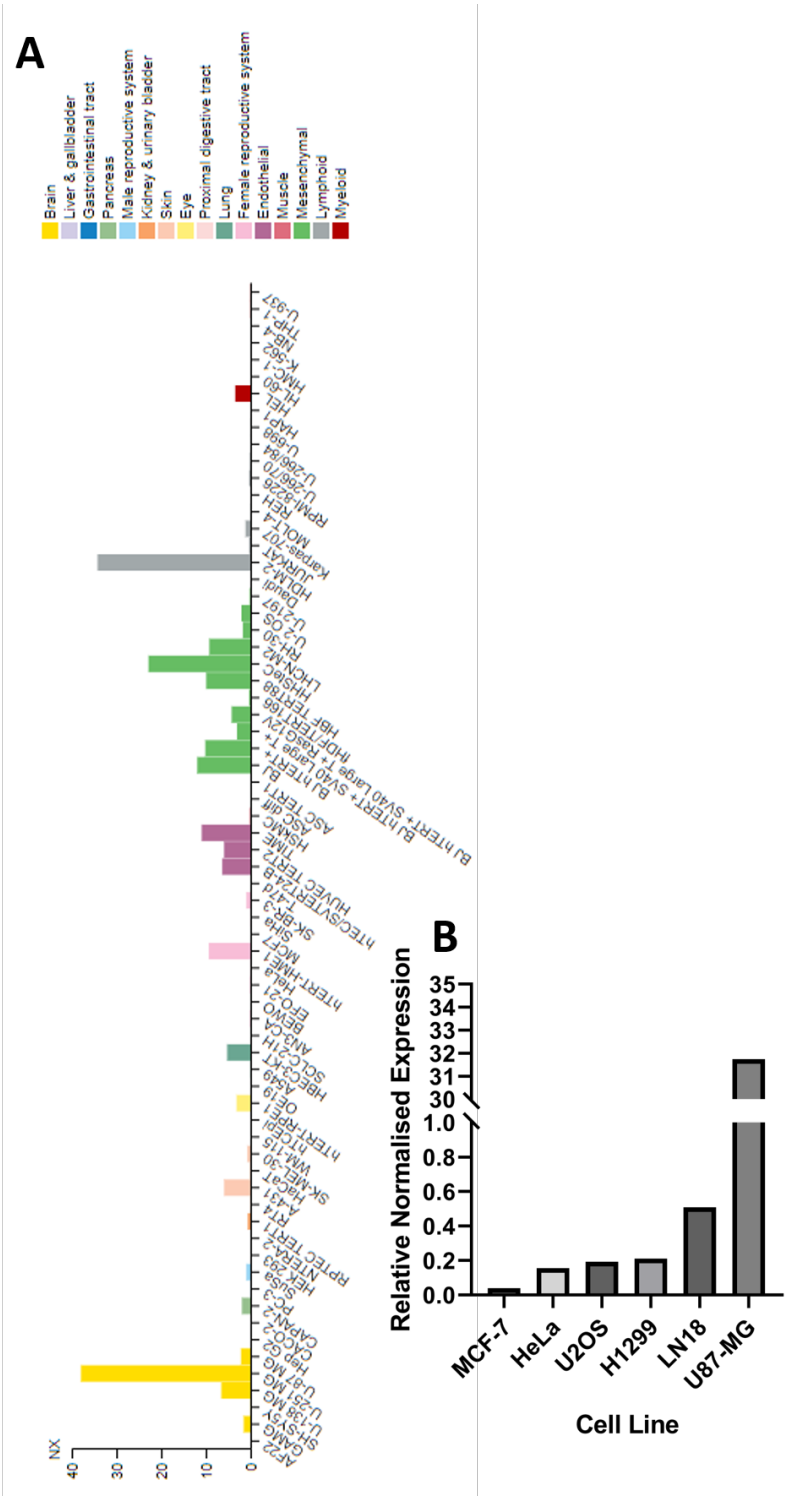

Figure 4.1: Cell Line Selection Process. (**A**) PD-L1 protein expression data in cell lines. Data taken from The Human Protein Atlas, (**B**) RT-qPCR analyses of different cancer cell lines. Cells were harvested after reaching 80-90% confluency, total cell RNA was extracted, and 100 ng of RNA was used in each reaction containing PD-L1 primers. RT-qPCR reactions were analysed using the Roche 480 Lightcycler. Results were normalised to β-Glucuronidase (GUS-β). Data was graphed using Graphpad Prism software.

4.2 Developing PD-L1 Staining Using PD-1/H2B Nucleosomal Arrays

To determine if the staining pattern of PD-1/H2B nucleosomal arrays was comparable to that of an antibody directed against PD-L1, the commercial DAKO 28:8 monoclonal antibody was used to stain both MCF-7 and U87-MG cells. This antibody is used in IHC assays to determine if patients are viable for PD-L1 immunotherapy (Cogswell et al., 2017) and recognises the extracellular domain of PD-L1 (Phe19-Thr239).

U87-MG and MCF-7 cells were both grown to 80-90% confluency before being fixed and incubated with DAKO 28:8 PD-L1 antibody at a concentration of 2.85 µg/mL. Antibody staining was then detected by immunofluorescence (see Section **2.7**). Representative images of both U87-MG and MCF-7 cells (Figure 4.2) show that PD-L1 expression is localised to the surface of the cell, and not within the cytoplasm or nucleus of the cell in Figure 4.2B or Figure 4.2F. While the general trend is that U87-MG cells show slightly higher fluorescence than MCF-7 cells (Figure 4.2D and 4.2F), it is not clear from this staining. Other fields of MCF-7 and U87-MG cells can be seen in Figure A.3 in the appendix.

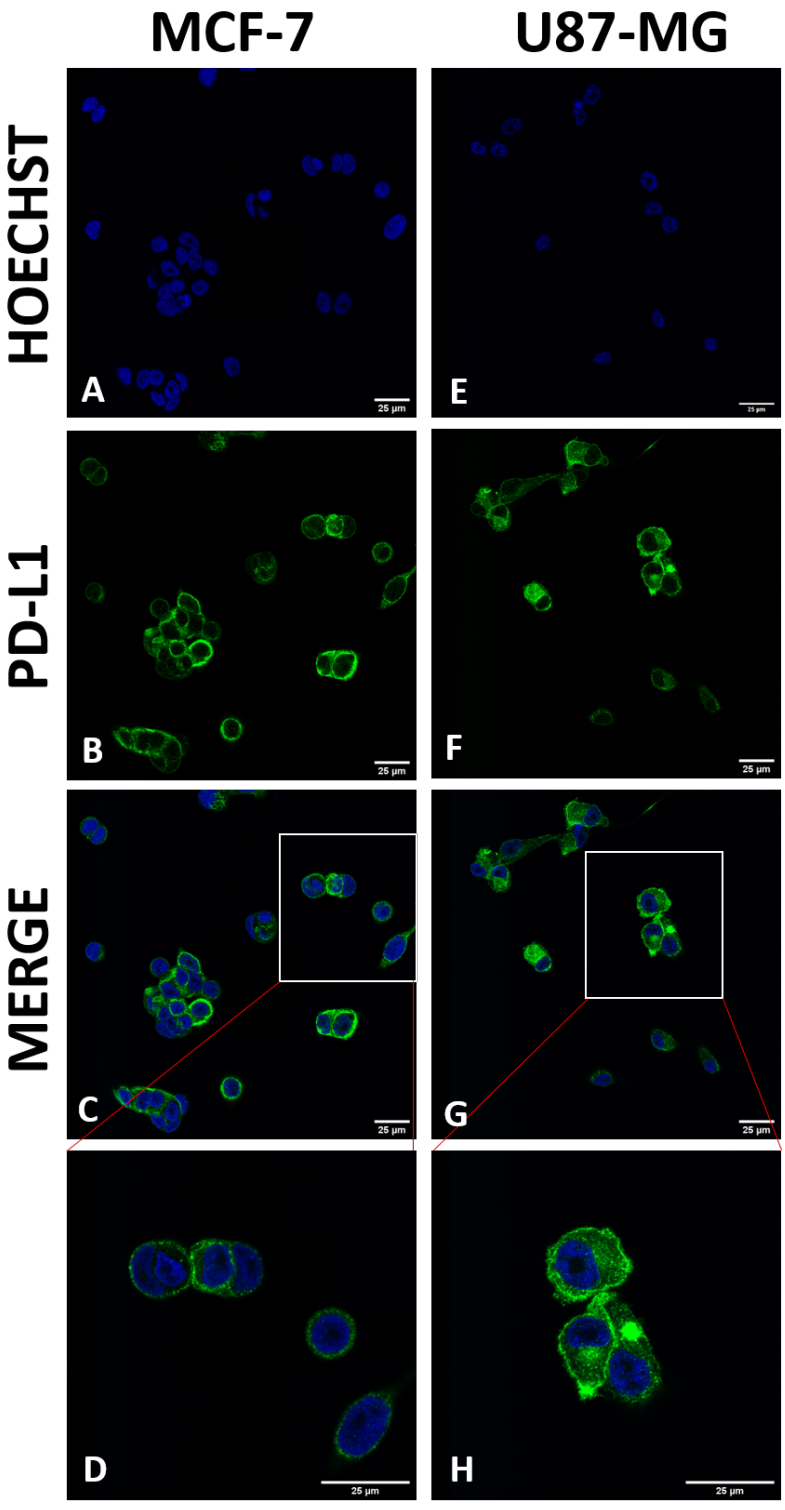

Figure 4.2: Immunofluorescence of MCF-7 and U87-MG Cells. MCF-7 cells (A-D) and U87-MG cells (E-H) were incubated with 2.85 µg/mL of PD-L1 antibody (green) overnight at 4°C with rocking, after which they were washed and incubated with anti-rabbit Alexa 555 to detect PD-L1 antibody and 1 µg/mL of Hoechst 33342 (blue) to stain nuclear DNA, (A & E), representative cell magnified 2.5x of (C & G), scale bar: 25 µm.

To test if the PD-1/H2B nucleosomal array binds specifically to PD-L1 on the surface of U87-MG and MCF-7 cells, the cells were grown to 80-90% confluency before being harvested and fixed. After fixation, cells were incubated with 1 µg of PD-1/H2B nucleosomal array for 1 hour at room temperature and stained with 2 µg of Avidin-488 conjugate to bind to biotin-labelled nucleosomal array DNA, or 2 µg of Avidin-488 conjugate alone for 30 minutes at room temperature in the dark to avoid photo-bleaching. Hoechst 33342 was used to stain nuclear DNA as it is water soluble and cell permeable, thus permeabilisation of the cells was not required (see Section **2.7.3**).

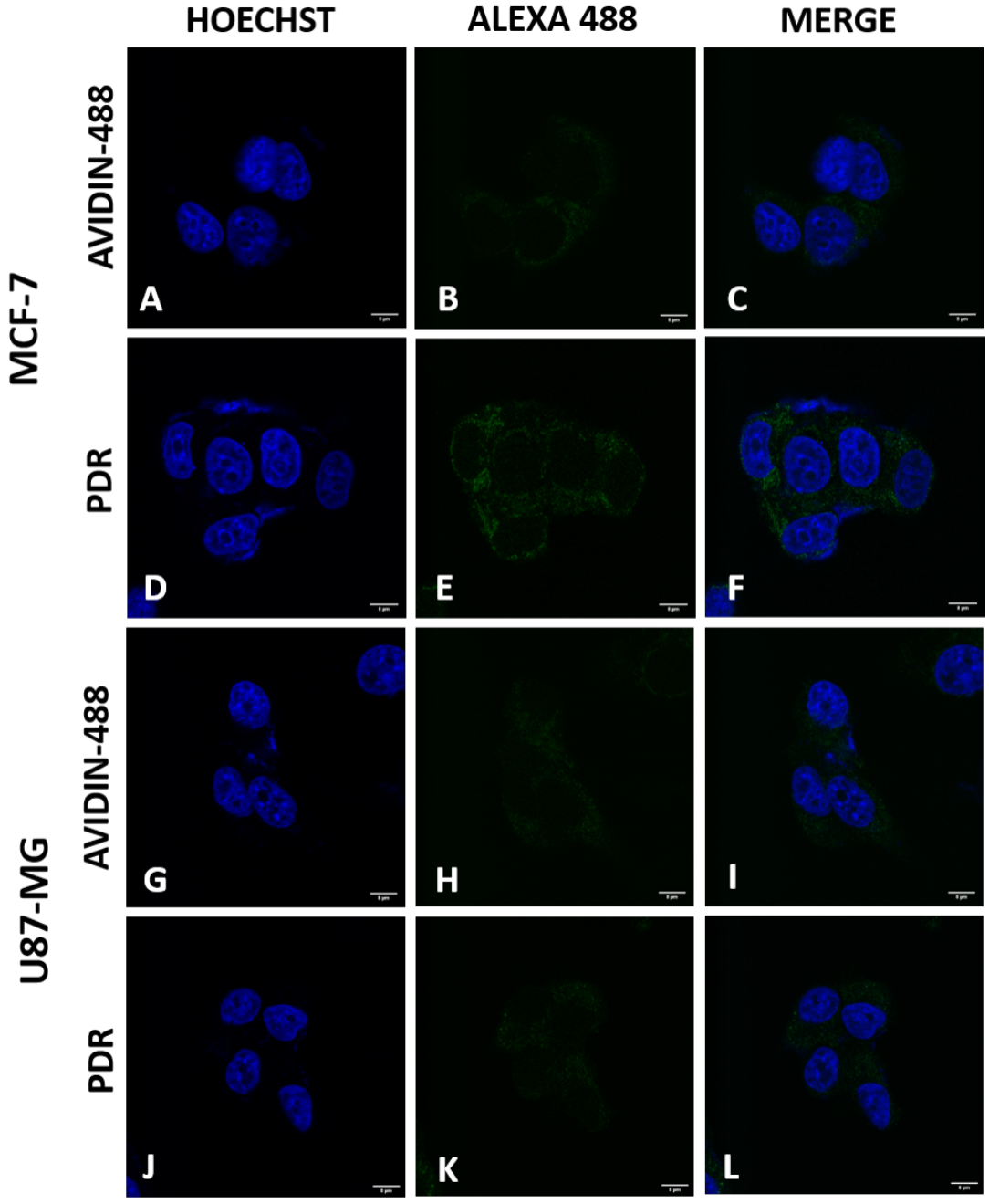

Figure 4.3: Avidin 488 Conjugate Binds Non-Specifically to the Outside of MCF-7 and U87-MG Cells. Fluorescence images of U87-MG and MCF-7 cells incubated with either 2 µg of Avidin 488 Conjugate or 1 µg of PD-1/H2B assembly and 488 conjugate. Nuclear DNA was stained with 1 µg/mL of Hoechst 33342 and PD-1/H2B arrays were visualised using Avidin 488 conjugate. In the merged images, DNA is blue and Avidin 488 conjugate is green, scale bar: 25 µm. PDR, PD-1/H2B nucleosomal arrays.

Figure 4.3 shows no detectable difference in staining intensity or localisation between MCF-7 cells incubated with Avidin-488 conjugate only (Figure 4.3B) and PD-1/H2B nucleosomal array (Figure 4.3E) as the staining intensity is low for MCF-7 cells incubated with Avidin-488 conjugate or PD-1/H2B nucleosomal arrays. As U87-MG cells incubated with Avidin-488 conjugate only (Figure 4.3H) and PD-1/H2B nucleosomal arrays (Figure 4.3K) resemble what is seen in MCF-7 cells, this indicates non-specific binding of the Avidin-488 conjugate to the surface of the cells.

As the results in Figure 4.3 showed no specific PD-1/H2B nucleosomal array binding in either cell line, it was questioned whether pre-incubation of PD-1/H2B nucleosomal arrays with Avidin-488 conjugate prior to staining of the cells removes background non-specific binding of Avidin-488 conjugate on the surface of the cell. Prior to incubating cell lines with PD-1/H2B nucleosomal array, 1 µg of nucleosomal array was incubated with 2 µg of Avidin-488 conjugate for 2 hours at room temperature in the dark. During this time, U87-MG and MCF-7 cells were fixed after which they were stained with Avidin-488 mixed PD-1/H2B assemblies, or Avidin-488 conjugate alone.

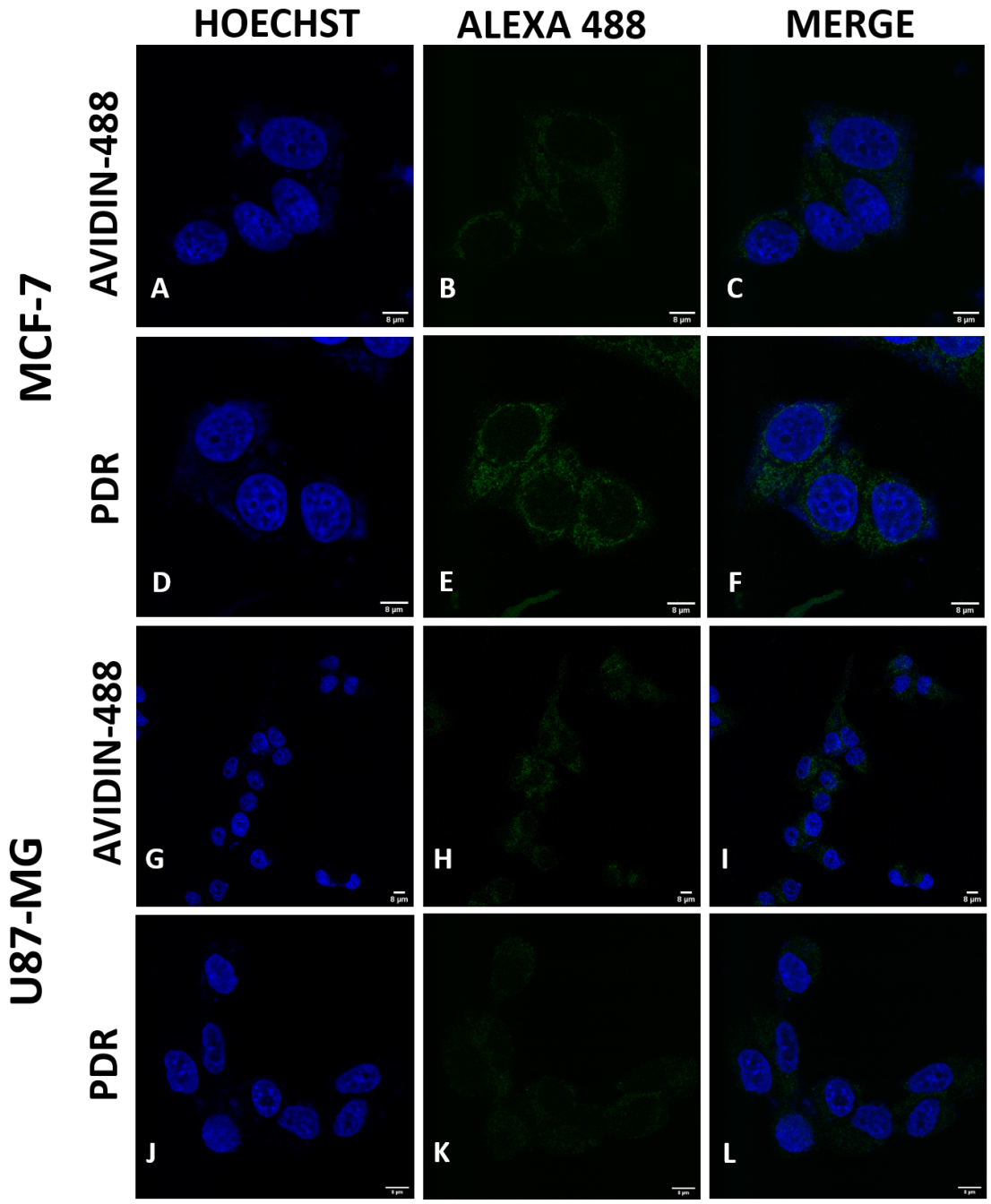

Figure 4.4: Incubation of Cells with Avidin-488 Pre-incubated PD-1/H2B Nucleosomal Arrays Results in Non-Specific Binding. Fluorescence images of U87-MG and MCF-7 cells incubated with either 2 µg of Avidin-488 conjugate or 1 µg of PD-1/H2B nucleosomal array (PDR). Nuclear DNA was stained with 1 µg/mL of Hoechst 33342 and Avidin-488 conjugate was used to detect biotin-labelled nucleosomal array DNA. In the merged images, DNA is blue and Avidin-488 conjugate is green, scale bar: 25 µm. PDR, PD-1/H2B nucleosomal arrays.

Figure 4.4 shows no detectable difference in staining intensity or localisation between MCF-7 cells incubated with Avidin-488 conjugate only (Figure 4.4B) and PD-1/H2B nucleosomal array (Figure 4.4E) as the staining intensity is low for MCF-7 cells incubated with Avidin-488 conjugate or PD-1/H2B nucleosomal arrays (Figure 4.4E). U87-MG cells incubated with PD-1/H2B assemblies do not show specific localisation of PD-1/H2B arrays (Figure 4.4K) as they closely resemble cells incubated with Avidin-488 conjugate alone (Figure 4.4H). Further to this, there is no difference in intensity between MCF-7 and U87-MG cells stained with PD-1/H2B assemblies, though U87-MG cells would be expected to have higher PD-L1 expression. While these results do not show significant changes from that of the previous experiment in which cells were incubated with PD-1 assemblies before being stained with Avidin-488 conjugate (Figure 4.3), pre-incubation of PD-1/H2B nucleosomal arrays was used during the remainder of the study to fluorescently label the PD-1/H2B nucleosomal arrays before applying them to cells.

As there remained non-specific binding of Avidin-488 conjugate, herring sperm DNA was used as a non-specific competitor to reduce background staining (Lee et al., 2015). As U87-MG cells highly express PD-L1, these cells were fixed and incubated with 100 µg/mL of herring sperm DNA in blocking buffer for 30 minutes, and then incubated with 1 µg of either DNA, Avidin-488 conjugate, WT or PD-1/H2B assemblies all of which were pre-incubated with 2 µg of Avidin-488 conjugate (see Section **2.7.3**).

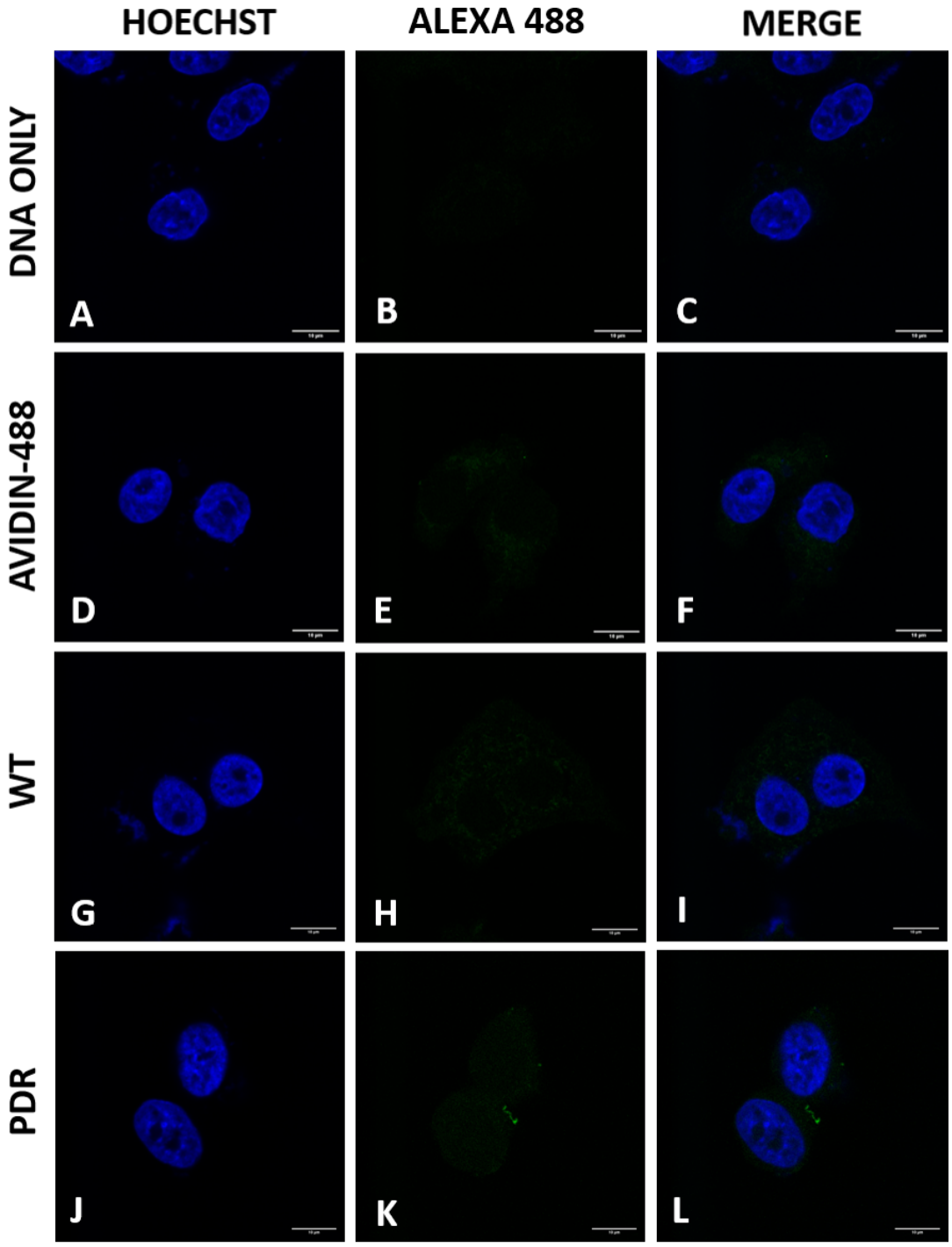

Figure 4.5: Herring Sperm Disrupts Both WT and PD-1/H2B Arrays Binding to U87-MG Cells. Fluorescence images of U87-MG cells incubated with 100 µg/mL of herring sperm DNA and 1 µg of biotin labelled pUC19 DNA, 2 µg of Avidin-488 conjugate, 1 µg of WT assembly, or 1 µg of PD-1/H2B nucleosomal array (PDR). Nuclear DNA was stained with 1 µg/mL of Hoechst 33342 and Avidin-488 conjugate was used to visualise biotin-labelled nucleosomal array DNA. In the merged images, DNA is blue and Avidin-488 conjugate is green, scale bar: 25 µm. PDR, PD-1/H2B nucleosomal arrays.

As seen in Figure 4.5, incubation of U87-MG cells with herring sperm DNA resulted in little discernible background staining in the Avidin-488 channel when U87-MG cells were incubated with the biotin labelled pUC19 DNA. Staining intensity was low on U87-MG cells incubated with Avidin-488 only (Figure 4.5E) and WT nucleosomal array (Figure 4.5H) as the octamers contain untagged H2B. However, herring sperm DNA also abrogates binding of PD-1/H2B nucleosomal arrays to cells (Figure 4.5K). This lack of staining indicates that the PD-1/H2B array did not bind to PD-L1 on the cell surface. The reason it is possibly due to the addition of the non-specific competitor, and hence herring sperm DNA was not be used in further assays.

As addition of herring sperm DNA hindered PD-1/H2B array binding, the washing buffer components were investigated next. In Figure 4.2, cells were washed with a PBS buffer containing 0.1% Triton X-100, a non-ionic detergent. It was hypothesised that the buffer may be too harsh to allow PD-1/H2B arrays to remain bound on the outside of the cell. Hence it was investigated whether the absence of this detergent in the wash buffer increases PD-1/H2B nucleosomal array binding to PD-L1 on the outside of MCF-7 and U87-MG cells. Both cells lines were incubated with PD-1/H2B assemblies and WT assemblies pre-mixed with Avidin-488 conjugate, or Avidin-488 conjugate alone for 1 hour at room temperature in the dark. After incubation, cells were only washed with PBS once after staining and fixed again (see Methodology **2.7.3**). Figures 4.6 and 4.7 show the brightfield and fluorescence images captured for both MCF-7 and U87-MG cells respectively.

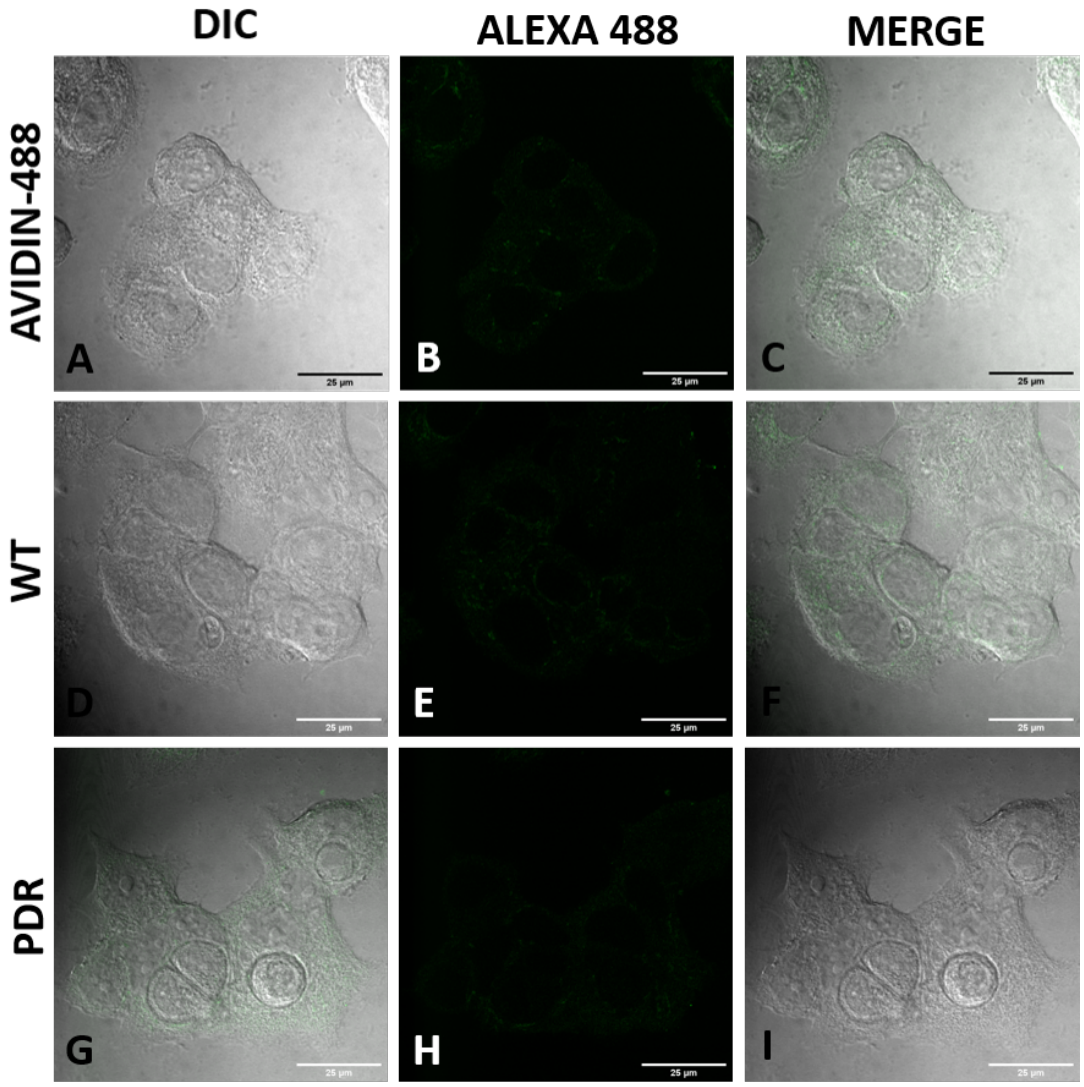

Figure 4.6: PDR Nucleosomal Arrays do not Detect PD-L1 on the Outside of MCF-7 Cells. Fluorescence images of MCF-7 cells incubated with 2 µg of Avidin 488 conjugate, 1 µg of WT assembly, or 1 µg of PD-1/H2B nucleosomal array (PDR). After fixation and mounting, cells were imaged in brightfield DIC (left) and Avidin-488 was used to detect biotin-labelled nucleosomal array DNA. Merged images show PDR assembly as green, scale bar: 25µm. PDR, PD-1/H2B nucleosomal arrays.

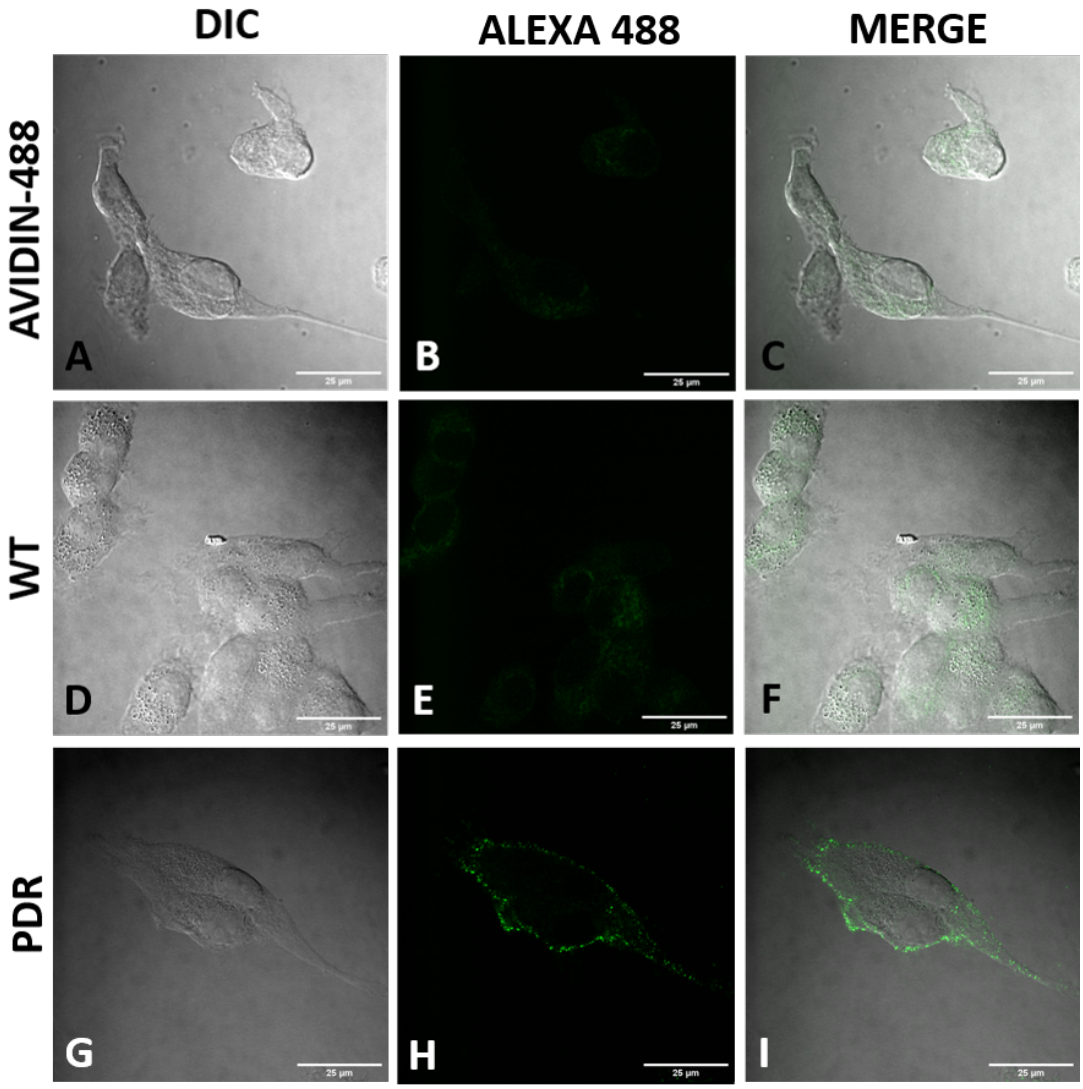

Figure 4.7: PDR nucleosomal Arrays Bind Detect PD-L1 on the Outside of U87-MG Cells. Fluorescence images of U87-MG cells incubated with 2 µg of Avidin 488 conjugate, 1 µg of WT assembly, or 1 µg of PD-1/H2B nucleosomal array (PDR). After fixation and mounting, cells were imaged in brightfield DIC (left) and Avidin-488 was used to detect biotin-labelled nucleosomal array DNA. Merged images show PDR assembly as green, scale bar: µm. PDR, PD-1/H2B nucleosomal arrays.

Figure 4.6 shows that for MCF-7 cells, there is no discernible staining between cells incubated with either Avidin 488 (Figure 4.6B), WT assembly (Figure 4.6E), or PD-1/H2B assembly (Figure 4.6H). It can therefore be concluded that there is non-specific binding of PD-1/H2B array to PD-L1 on the cell surface of MCF-7

cells, even without detergent in the wash buffer. However, there was no non-specific binding of the Avidin-488 conjugate. Other fields of cells are shown in Figure A.4.

Figure 4.7 shows representative images of U87-MG cells treated in the same fashion as MCF-7 cells in Figure 4.6. The lack of staining in Figures 4.7B and 4.7E indicate there is no specific binding of either Avidin 488 alone, or WT assembly which is what is expected as neither contain a PD-1 peptide to bind to PD-L1. However, Figure 4.7H, however, shows a distinct staining pattern of punctate foci on the surface of the cells. The merged image (Figure 4.7I) illustrates that this staining is not present within either in the cytoplasm or the nucleus (other fields of cells are shown in Figure A.3). This would indicate that PD-1/H2B array bound specifically to the outside of high PD-L1 expressing U87-MG cells and that nucleosomal arrays are able to detect differential PD-L1 expression between cell lines as MCF-7 cells lacked this staining. This staining pattern is distinguishable from either negative control WT nucleosomal arrays and the Avidin-488 conjugate alone. Therefore PD-1/H2B nucleosomal arrays can detect PD-L1 on the surface of U87-MG cells. Other fields of cells are shown in Figure A.5.

4.3 Using PD-1/H2B Nucleosomal Arrays in Other Assays

The use of the PD-1/H2B nucleosomal arrays in other formats was also tested. However, due to time constraints, this was unable to be completed. Initially fluorescence was measured using the Roche 480 Lightcycler as a high throughput method that enabled fast detection. U87-MG cells were harvested and incubated with a range of differing amounts (0.5 µg to 5 µg) of either PD-1/H2B assembly, or WT nucleosomal arrays assembled with Cy5-labelled pUC19 DNA. As shown in Figure 4.7, U87-MG cells incubated with higher amounts of Cy5 PD-1/H2B assembly emitted greater fluorescence than those cells stained with WT nucleosomal arrays. This indicates that not only is the emitted fluorescence from the array able to be captured, but that the fluorophore-labelled PD-1/H2B binds to cells through the PD-L1/PD-1 interaction as any unbound assembly was removed through a series of washing steps. The more PD-1/H2B assembly that is added

to the cells, the greater the fluorescence capture. This is especially noticeable with those cells incubated with 5 µg of this assembly. This may further indicate that there is a 'minimum' amount of array needed in order to bind PD-L1 on the surface of tumour cells, and to detect a significant difference between stained and unstained cells. Given that this assay was done with Cy5 labelled DNA that does not form properly spaced nucleosomes (Figure 3.13), this assay needs to be repeated with PD-1/H2B nucleosomal arrays made with biotin-Avidin-488 labelled DNA. WT assembly made using Cy5-labelled pUC19 plasmid DNA.

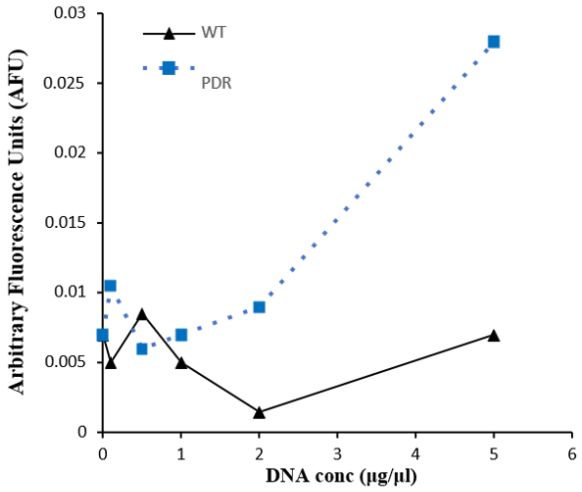

Figure 4.8: PD-1/H2B-Cy5 Nucleosomal Arrays Bind Selectively to U87-MG Cells. U87-MG cells were re-suspended at a density of 5 x 10^6 cells/mL, after which 0, 0.1 µg, 0.5 µg, 1 µg, 2 µg, or 5 µg of Cy5-PD-1/H2B nucleosomal array or Cy5-Wild Type nucleosomal array was applied. U87-MG cells were incubated at room temperature in the dark for 2 hours, after which they were washed and 20 µL of each reaction was transferred to a 96 well plate. Fluorescence was captured using the Roche 480 Light Cycler using the Cy5 filter (615 nm - 670 nm). The program for this assay is detailed in Section **2.8.1**.

Fluorescence activated cell sorting (FACS) was also used to test whether there was a detectable difference in the fluorescence capture of PD-1/H2B nucleosomal arrays made with Cy3-labelled DNA between high and low PD-L1 expressing tumour cell lines U87-MG and MCF-7 cells respectively. These cell lines were harvested and 5 x 10^4 of cells were incubated with either with 0.1 µg, 0.5 µg or 1 µg of PD-1/H2B-Cy3 nucleosomal arrays for two hours after which fluorescent cell populations were separated using FACS. The PE filter was used to detect the Cy3 fluorophore, and the FITC filter was used to capture any fluorescence

emitted at a lower wavelength.

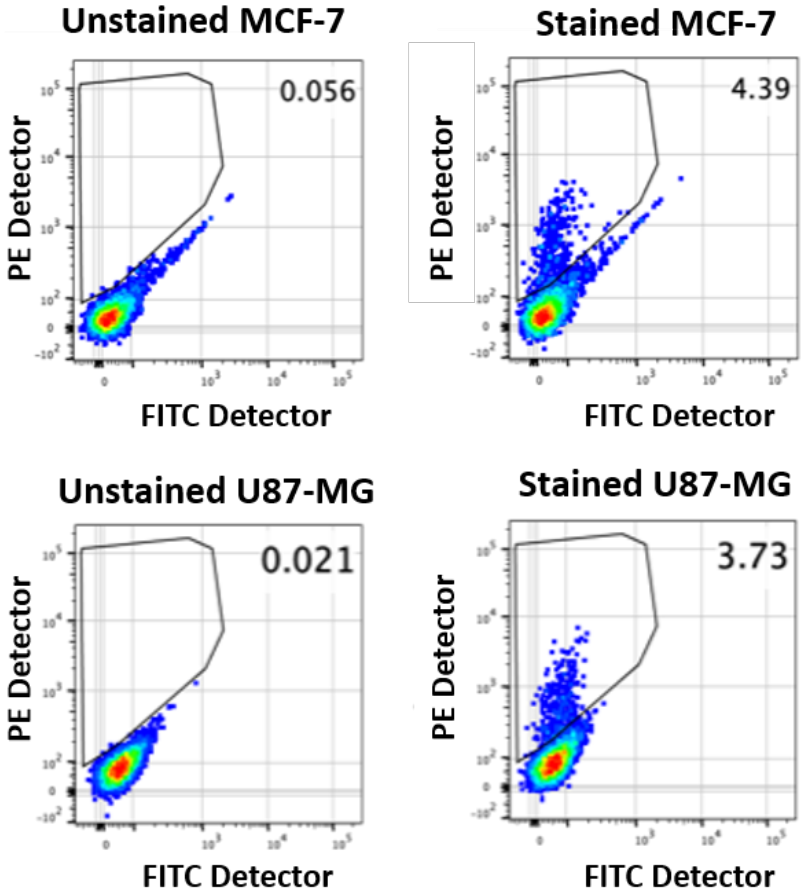

Figure 4.9: Differences Between Stained and Unstained Cell Populations are Indistinguishable Using FACS. U87-MG and MCF-7 cells were grown to 80-90% confluency and resuspended at a density of 5.0 x 10^5 cells/mL. Cells were left unstained or incubated with 1 µg of Cy3-PD-1/H2B arrays for 30 minutes and fixed, after which cell populations were separated using FACS. These are indicated by the gates on the left of each image. PE: R-phycoerythrin filter (Ex 566 nm Em 574), FITC: fluorescein filter (Ex 490 nm, Em 525 nm).

Analysis of stained and unstained MCF-7 and U87-MG cell populations revealed no significant difference either between Cy3-PD-1/H2B nucleosomal array stained cells and unstained cells, or between cell lines. Unstained cells used as negative controls revealed that only a small fraction of unstained MCF-7 (0.056%) and U87-MG (0.021%) of cells emitted detectable fluorescence as shown in the gates. However, 4.4% of stained MCF-7 cells and 3.7% of U87-MG cells stained positive for the Cy3 fluorophore (PE detector). The small percentage of stained cells

suggests that the PD-1/H2B nucleosomal arrays did not bind to PD-L1 on the surface of the cells. These results indicate that the cells may need longer incubation time with the array, or more of the array in order to observe a detectable difference in cell populations.

As Cy3 and Cy5 labelled DNA was the only labelling system available in the laboratory at the time, it was used to assemble the nucleosomal arrays used above. Subsequently, as shown in Figure 3.12 and Figure 3.13, it was determined that the Cy3 and Cy5-labelled arrays do not form properly spaced nucleosomes. These protocols still requires further optimisation. Initially, biotin-PD-1/H2B arrays will be used alongside WT assemblies and Avidin-488 only negative controls. After being optimised in U87-MG cells, these assays would then be performed on MCF-7 cells to detect whether there is differential binding of PD-1/H2B arrays between low and high PD-L1 expressing cell lines.

Chapter 5

Discussion and Future Directions

5.1 Forming Peptide Tagged Nucleosomal Arrays

This research investigated whether the core histone H2B, with a receptor domain at its N-terminal tail could, along with the other core histones and fluorescently labelled DNA, form a nucleosomal array and whether this then binds to a ligand on the cell surface and be detected. This is a high affinity interaction that should increase specificity than that of antibodies.

As proof of principle, this study utilised the reaction that occurs endogenously between PD-L1 and PD-1 by incorporating the extracellular domain of PD-1, which binds to PD-L1, on the N-terminal tail of histone H2B. Accurately determining the presence of PD-L1 on the surface of cells is of importance as PD-L1 over-expression is used as a predictive bio-marker to determine whether patients are viable for PD-L1/PD-1 immunotherapy. IHC assays are the standard diagnostic method to determine PD-L1 expression levels on patient histological samples. However, the PD-L1 antibody used varies between diagnostic laboratories, and the performance of these antibodies also differs greatly (Torlakovic et al., 2020; Kintsler et al., 2019; Schats et al., 2018). Using the PD-1 extracellular domain to detect the level of PD-L1 on cancer cells should overcome this issue.

A protocol for fluorescent confocal microscopy was developed to test if PD-1 containing array bound specifically to the surface of U87-MG cells. PD-1/H2B containing nucleosomal arrays bound specifically to the surface of U87-MG cells while control WT nucleosomal arrays and Avidin-488 alone did not adhere to the surface of cells. PD-1/H2B nucleosomal arrays did not bind to the surface of MCF-7 cells, indicating that these arrays were able to differentially detect PD-L1 expression levels between cell lines. It was necessary for biotin to be pre-bound with Avidin-Alexa-488. When added after PD-1/H2B nucleosomal arrays were incubated with cells, there was non specific background staining. Thus, pre-incubating assemblies first and washing away excess reduced background non-specific binding. Coupling this method with washing cells in a non-ionic detergent wash buffer also improved staining intensity.

Though the presence of the PD-1 peptide tag on the N-terminal tail of histone H2B did not affect nucleosomal array formation, the method of fluorescently labelling DNA was important. Using biotin labelled DNA had correct nucleosome

phasing whereas using Cy3 or Cy5 labelled DNA did not work as nucleosomes were not positioned properly. Studies have shown that Cy3 and Cy5 fluorophores when present in the DNA prevented DNA bending. They have high affinity to TA base pairs which lie in the minor groove of DNA where there is greater distortion of DNA that is energetically unfavourable (Balasubramanian et al., 2009; Morozov et al., 2009). The fluorophore acts as an additional base pair that straightens DNA and reduces the ability of other base pairs to roll freely (Spiriti et al., 2011). As the Widom sequence contains these TA base pairs to allow it to bend and position nucleosomes, labelling with Cy3 or Cy5 likely hinders this ability. This is the probable reason for the lack of properly phased nucleosomes and nucleosome formation that was encountered when using these fluorophores.

5.2 Benefits of Nucleosomal Arrays

Nucleosomal arrays can vary in length with the number of nucleosomal repeat sequences in the array. The nucleosomal arrays formed in this study contain two H2B histone proteins per unit and so contain 32 potential binding sites for PD-L1. This increases the ability to detect PD-L1 on the surface of cells. IgG antibodies have only two epitope binding sites (Janeway Jr et al., 2001). As the nucleosomal arrays formed in this study all contain the same receptor-tagged H2B, these assemblies will only recognise PD-L1 on the surface of the cells. Further to this, the ability to label the DNA at multiple sites allows greater signal amplification rather than a fluorophore-conjugated primary or likely fluorophore-conjugated secondary antibody. In addition, nucleosomal arrays are relatively easy to produce whereas antibody production can be expensive.

However, using PD-1/H2B nucleosomal arrays to detect protein on the surface of a cell still has the same staining and scoring issues the IHC assays. The staining pattern could depend on the preparation of samples and the formation of the nucleosomal arrays. Further to this, different scoring matrices between diagnostic laboratories may give different conclusions of whether patients need to undergo PD-L1/PD-1 immunotherapy. Future optimisations may help reduce these concerns with further improvements on nucleosomal array formation and enhanced staining protocols.

Currently there are two commercially available PD-L1 IHC assay kits (Ventana PD-L1 Assay, Roche Diagnostics and PD-L1 22C3, pharmDx, Aligent) each with their own scoring algorithm and protocol, with different PD-L1 antibodies utilised in the assay. These antibodies recognise different PD-L1 splicing variants, some of which may be preferentially present in different tumour types. Not all PD-L1 antibodies used in the diagnostic IHC assays are able to recognise different PD-L1 splicing variants expressed on a patient histological sample. This suggests that PD-L1 IHC assays are not interchangeable, and can pose a risk to patient health if it is concluded that they are not viable for PD-L1-PD-1 immunotherapy based on which IHC assay was used.

Other PD-L1 isoforms exist that are secreted from the cell and homo-dimerise. Studies investigating this phenomenon have shown the addition of an 18 amino acid domain facilitates bending and homo-dimerization (Mahoney et al., 2019). This secreted form of PD-L1 has also been shown to correlate with clinically aggressive non-small cell lung cancer and renal cell carcinoma (Takeuchi et al., 2018; Frigola et al., 2011). Not all PD-L1 antibodies used in IHC will be able to recognise this secreted form of PD-L1. PD-1/H2B nucleosomal arrays are able to overcome this issue as different fragments of the PD-1 receptor are able to be fused to different histone N-terminal tails. This would allow the nucleosomal arrays to detect secreted PD-L1 and different PD-L1 splicing variants unlike a monoclonal PD-L1 antibody.

5.3 Future Directions

To confirm that these nucleosomal arrays are able to detect differential PD-L1 expression on cancer cells, the assemblies need to be tested on a range of cells lines with known PD-L1 expression. Future optimisations will include testing PD-1/H2B nucleosomal arrays on other cell lines. This will help further demonstrate that these nucleosomal arrays are able to detect differential PD-L1 expression on cancer cells sourced from other tumour types. Nucleosomal array formation may be further optimised by investigating the dialysis buffer used to form the assemblies. All nucleosomal assemblies made in this study were dialysed in NaCl gradient buffers. Including K^+ and Mg^{2+} abrogates formation of the 30 nm

chromatin fibre (Allahverdi et al., 2015) and dialysing nucleosomal assemblies in different ionic buffers, or a mixture of ionic buffers, should be investigated in the future. This may also help with the visualisation of the nucleosomal arrays using TEM.

5.3.1 Optimising the Detection of PD-L1

In this study, only histone H2B was tagged with the extracellular domain of PD-1. In the future, nucleosomal arrays could be formed with all histones tagged with PD-1. Forming nucleosomal arrays that contain all the core histones tagged within the histone octamers may increase the binding to PD-L1 on the cell surface. If the same number of repeats of the nucleosome positioning sequence is used, this increases the number of potential binding sites to 128. No evidence suggests that PD-1 homo-dimerises (Zak et al., 2015) and therefore it can be assumed that this peptide tag would not be the cause of aggregation in these nucleosomal arrays. Histone H2B N-terminal tails are needed for proper H2A/H2B dimer formation and therefore nucleosome formation (Thiriet and Hayes, 2001; Mao et al., 2016). Not only does tagging H2B N-terminal tails have no adverse effects on nucleosomal array formation, the other core histone N-terminal tails are dispensable for compaction (de la Barre et al., 2001). In the future, decreasing or increasing the number of Widom sequence repeats will be investigated. Increasing the number of tagged histones may require a smaller number of Widom 601 repeats. It may be that using both PD-1 tagged H2A/H2B dimers and a shorter nucleosomal array improves binding and prevents aggregation, and a more significant difference may be detected between different cell lines. As the same plasmid will be used, the biotin-labelling should not be greatly reduced so signal amplification would not decrease.

It has been well established that over-expression of PD-L1 is linked to poor prognosis of cancer patients while there is less evidence to suggest that PD-L2 expression is associated with patient prognosis compared to PD-L1. Interestingly, PD-L2 binds to PD-1 with three times higher affinity than PD-L1 and yet PD-L1 and PD-L2 share only 39% amino acid identity. It is speculated higher affinity is due to the presence of a tryptophan residue at position 110 (W110) rather than an alanine at position 121 in PD-L2 and PD-L1 respectively (Viricel et al., 2015).

Some reports have noted the tryptophan replacement weakens affinity of PD-L2 to PD-1, and that affinity in increased due to the presence of a flexible loop region that latches onto PD-1, preventing W110 from inhibiting the interaction (Philips et al., 2020). As this interaction is much stronger than that of PD-L1 to PD-1, it would be interesting to investigate whether PD-1/H2B nucleosomal arrays also to bind to PD-L2 on the surface of cancer cells.

5.4 Other Platforms for Detection

This PD-1/H2B nucleosomal array also needs to be optimised for use in other formats. For example, FACS can be developed for cells in suspension with arrays containing the Alexa-488-biotin assemblies, as per Figure 4.9, with appropriate controls and duplicates. Other assays that use different formats for detecting the fluorescence of this nucleosomal assembly can be developed such as those that use plate readers to detect fluorescence and this would develop a high-throughput screening method for PD-L1 expression.

The success of using the PD-L1/PD-1 endogenous interaction in these nucleosomal arrays is indicative that alternate nucleosomal arrays could be formed that target other extracellular proteins. A previous study used nucleosomal arrays to display a Ras peptide to determine whether this raised an antibody response in mouse models (Parlane et al., 2020). There was no disruption to nucleosomal array formation when the Ras peptide was attached to all core histone N-terminal tails. Although non-immunogenic, this does show that different nucleosomal arrays can be formed with alternate peptides.

5.5 Summary

This study has shown that nucleosomal arrays are able to be formed with PD-1 receptor tagged H2B N-terminal tails and these arrays are able to be fluorescently labelled using Avidin-Alexa-488-biotin. It was shown that tagging the N-terminal tail of core histone H2B does not affect nucleosome formation but that the method of fluorescently labelling the positioning DNA is important. A staining protocol

was developed to demonstrate that the PD-1/H2B nucleosomal assemblies bind to PD-L1 on the surface of U87-MG and that they detect differential expression between cell lines. As this study used the high affinity endogenous PD-L1/PD-1 interaction, it suggests that this system could also be used to detect other extracellular proteins, and further development may result in an alternate staining technique to antibody based assays.

Bibliography

Alifieris, C. and Trafalis, D. T. (2015). Glioblastoma multiforme: Pathogenesis and treatment. *Pharmacology & therapeutics*, 152:63–82.

Allahverdi, A., Chen, Q., Korolev, N., and Nordenskiöld, L. (2015). Chromatin compaction under mixed salt conditions: opposite effects of sodium and potassium ions on nucleosome array folding. *Scientific reports*, 5(1):1–7.

Arents, G., Burlingame, R. W., Wang, B.-C., Love, W. E., and Moudrianakis, E. N. (1991). The nucleosomal core histone octamer at 3.1 a resolution: a tripartite protein assembly and a left-handed superhelix. *Proceedings of the National Academy of Sciences*, 88(22):10148–10152.

Arents, G. and Moudrianakis, E. N. (1995). The histone fold: a ubiquitous architectural motif utilized in dna compaction and protein dimerization. *Proceedings of the National Academy of Sciences*, 92(24):11170–11174.

Balasubramanian, S., Xu, F., and Olson, W. K. (2009). Dna sequence-directed organization of chromatin: structure-based computational analysis of nucleosome-binding sequences. *Biophysical journal*, 96(6):2245–2260.

Baldi, S., Korber, P., and Becker, P. B. (2020). Beads on a string—nucleosome array arrangements and folding of the chromatin fiber. *Nature structural & molecular biology*, 27(2):109–118.

Bannister, A. J. and Kouzarides, T. (2011). Regulation of chromatin by histone modifications. *Cell research*, 21(3):381–395.

Barrow, A. D. and Trowsdale, J. (2006). You say itam and i say itim, let's call the whole thing off: the ambiguity of immunoreceptor signalling. *European journal of immunology*, 36(7):1646–1653.

Berghoff, A. S., Kiesel, B., Widhalm, G., Rajky, O., Ricken, G., Wöhrer, A., Dieckmann, K., Filipits, M., Brandstetter, A., Weller, M., et al. (2015). Programmed death ligand 1 expression and tumor-infiltrating lymphocytes in glioblastoma. *Neuro-oncology*, 17(8):1064–1075.

Buchbinder, E. I. and Desai, A. (2016). Ctla-4 and pd-1 pathways: similarities, differences, and implications of their inhibition. *American journal of clinical oncology*, 39(1):98.

Butte, M. J., Keir, M. E., Phamduy, T. B., Sharpe, A. H., and Freeman, G. J. (2007). Programmed death-1 ligand 1 interacts specifically with the b7-1 costimulatory molecule to inhibit t cell responses. *Immunity*, 27(1):111–122.

Coca, S., Perez-Piqueras, J., Martinez, D., Colmenarejo, A., Saez, M. A., Vallejo, C., Martos, J. A., and Moreno, M. (1997). The prognostic significance of intratumoral natural killer cells in patients with colorectal carcinoma. *Cancer: Interdisciplinary International Journal of the American Cancer Society*, 79(12):2320–2328.

Cogswell, J., Inzunza, H. D., Wu, Q., Feder, J. N., Mintier, G., Novotny, J., and Cardona, D. M. (2017). An analytical comparison of dako 28-8 pharmdx assay and an e1l3n laboratory-developed test in the immunohistochemical detection of programmed death-ligand 1. *Molecular diagnosis & therapy*, 21(1):85–93.

de la Barre, A.-E., Angelov, D., Molla, A., and Dimitrov, S. (2001). The n-terminus of histone h2b, but not that of histone h3 or its phosphorylation, is essential for chromosome condensation. *The EMBO journal*, 20(22):6383–6393.

Diggs, L. P. and Hsueh, E. C. (2017). Utility of pd-l1 immunohistochemistry assays for predicting pd-1/pd-l1 inhibitor response. *Biomarker research*, 5(1):12.

Dunn, G. P., Old, L. J., and Schreiber, R. D. (2004). The three es of cancer immunoediting. *Annu. Rev. Immunol.*, 22:329–360.

Flaus, A. (2011). Principles and practice of nucleosome positioning in vitro. *Frontiers in life science*, 5(1-2):5–27.

Frigola, X., Inman, B. A., Lohse, C. M., Krco, C. J., Cheville, J. C., Thompson, R. H., Leibovich, B., Blute, M. L., Dong, H., and Kwon, E. D. (2011). Identification of a soluble form of b7-h1 that retains immunosuppressive activity

and is associated with aggressive renal cell carcinoma. *Clinical cancer research*, 17(7):1915–1923.

Garcia-Diaz, A., Shin, D. S., Moreno, B. H., Saco, J., Escuin-Ordinas, H., Rodriguez, G. A., Zaretsky, J. M., Sun, L., Hugo, W., Wang, X., et al. (2017). Interferon receptor signaling pathways regulating pd-l1 and pd-l2 expression. *Cell reports*, 19(6):1189–1201.

Gato-Cañas, M., Zuazo, M., Arasanz, H., Ibañez-Vea, M., Lorenzo, L., Fernandez-Hinojal, G., Vera, R., Smerdou, C., Martisova, E., Arozarena, I., et al. (2017). Pdl1 signals through conserved sequence motifs to overcome interferon-mediated cytotoxicity. *Cell reports*, 20(8):1818–1829.

Giaimo, B. D., Ferrante, F., Herchenröther, A., Hake, S. B., and Borggrefe, T. (2019). The histone variant h2a. z in gene regulation. *Epigenetics & chromatin*, 12(1):1–22.

Gowrishankar, K., Gunatilake, D., Gallagher, S. J., Tiffen, J., Rizos, H., and Hersey, P. (2015). Inducible but not constitutive expression of pd-l1 in human melanoma cells is dependent on activation of nf-κb. *PloS one*, 10(4):e0123410.

Guo, X.-W. and Cole, R. D. (1989). Chromatin aggregation depends on the anion species of the salts. *Journal of Biological Chemistry*, 264(28):16873–16879.

Gutcher, I. and Becher, B. (2007). Apc-derived cytokines and t cell polarization in autoimmune inflammation. *The Journal of clinical investigation*, 117(5):1119–1127.

Hanahan, D. and Weinberg, R. A. (2011). Hallmarks of cancer: the next generation. *cell*, 144(5):646–674.

Hao, C., Chen, G., Zhao, H., Li, Y., Chen, J., Zhang, H., Li, S., Zhao, Y., Chen, F., Li, W., et al. (2020). Pd-l1 expression in glioblastoma, the clinical and prognostic significance: A systematic literature review and meta-analysis. *Frontiers in Oncology*, 10.

Heins, J. N., Suriano, J. R., Taniuchi, H., and Anfinsen, C. B. (1967). Characterization of a nuclease produced by staphylococcus aureus. *Journal of Biological Chemistry*, 242(5):1016–1020.

Hodi, F. S., Chiarion-Sileni, V., Gonzalez, R., Grob, J.-J., Rutkowski, P., Cowey, C. L., Lao, C. D., Schadendorf, D., Wagstaff, J., Dummer, R., et al. (2018). Nivolumab plus ipilimumab or nivolumab alone versus ipilimumab alone in advanced melanoma (checkmate 067): 4-year outcomes of a multicentre, randomised, phase 3 trial. *The Lancet Oncology*, 19(11):1480–1492.

Janeway Jr, C. A., Travers, P., Walport, M., and Shlomchik, M. J. (2001). The structure of a typical antibody molecule. In *Immunobiology: The Immune System in Health and Disease. 5th edition*. Garland Science.

Kintsler, S., Cassataro, M. A., Drosch, M., Holenya, P., Knuechel, R., and Braunschweig, T. (2019). Expression of programmed death ligand (pd-l1) in different tumors. comparison of several current available antibody clones and antibody profiling. *Annals of diagnostic pathology*, 41:24–37.

Klein, L., Kyewski, B., Allen, P. M., and Hogquist, K. A. (2014). Positive and negative selection of the t cell repertoire: what thymocytes see (and don't see). *Nature Reviews Immunology*, 14(6):377–391.

Lee, J., Choi, K.-j., Choi, Y., Ali, B. A., Al-Khedhairy, A. A., and Kim, S. (2015). Sperm dna-mediated reduction of nonspecific fluorescence during cellular imaging with quantum dots. *Chemical Communications*, 51(58):11584–11586.

Leonard, W. J. and Lin, J.-X. (2000). Cytokine receptor signaling pathways. *Journal of Allergy and Clinical Immunology*, 105(5):877–888.

Lowary, P. and Widom, J. (1998). New dna sequence rules for high affinity binding to histone octamer and sequence-directed nucleosome positioning. *Journal of molecular biology*, 276(1):19–42.

Luger, K., Mäder, A. W., Richmond, R. K., Sargent, D. F., and Richmond, T. J. (1997). Crystal structure of the nucleosome core particle at 2.8 å resolution. *Nature*, 389(6648):251–260.

Mahoney, K. M., Shukla, S. A., Patsoukis, N., Chaudhri, A., Browne, E. P., Arazi, A., Eisenhaure, T. M., Pendergraft, W. F., Hua, P., Pham, H. C., et al. (2019). A secreted pd-l1 splice variant that covalently dimerizes and mediates immunosuppression. *Cancer Immunology, Immunotherapy*, 68(3):421–432.

Mao, P., Kyriss, M. N., Hodges, A. J., Duan, M., Morris, R. T., Lavine, M. D., Topping, T. B., Gloss, L. M., and Wyrick, J. J. (2016). A basic domain in the histone h2b n-terminal tail is important for nucleosome assembly by fact. *Nucleic acids research*, 44(19):9142–9152.

Marcus, A., Gowen, B. G., Thompson, T. W., Iannello, A., Ardolino, M., Deng, W., Wang, L., Shifrin, N., and Raulet, D. H. (2014). Recognition of tumors by the innate immune system and natural killer cells. In *Advances in immunology*, volume 122, pages 91–128. Elsevier.

Moon, J. W., Kong, S.-K., Kim, B. S., Kim, H. J., Lim, H., Noh, K., Kim, Y., Choi, J.-W., Lee, J.-H., and Kim, Y.-S. (2017). Ifnγ induces pd-l1 overexpression by jak2/stat1/irf-1 signaling in ebv-positive gastric carcinoma. *Scientific reports*, 7(1):1–13.

Morales, V. and Richard-Foy, H. (2000). Role of histone n-terminal tails and their acetylation in nucleosome dynamics. *Molecular and cellular biology*, 20(19):7230–7237.

Morozov, A. V., Fortney, K., Gaykalova, D. A., Studitsky, V. M., Widom, J., and Siggia, E. D. (2009). Using dna mechanics to predict in vitro nucleosome positions and formation energies. *Nucleic acids research*, 37(14):4707–4722.

Nakanishi, J., Wada, Y., Matsumoto, K., Azuma, M., Kikuchi, K., and Ueda, S. (2007). Overexpression of b7-h1 (pd-l1) significantly associates with tumor grade and postoperative prognosis in human urothelial cancers. *Cancer Immunology, Immunotherapy*, 56(8):1173–1182.

Ng, S., Yue, W., Oppermann, U., and Klose, R. (2009). Dynamic protein methylation in chromatin biology. *Cellular and Molecular Life Sciences*, 66(3):407–422.

Olins, A. L. and Olins, D. E. (1974). Spheroid chromatin units (ν bodies). *Science*, 183(4122):330–332.

Parlane, N. A., Wedlock, D. N., Han, J.-H., and Park, J. H. (2020). Heterologous peptide display on chromatin nanofibers: A new strategy for peptide vaccines. *Biochemical and biophysical research communications*, 524(4):825–831.

Parry, R. V., Chemnitz, J. M., Frauwirth, K. A., Lanfranco, A. R., Braunstein, I., Kobayashi, S. V., Linsley, P. S., Thompson, C. B., and Riley, J. L. (2005). Ctla-4 and pd-1 receptors inhibit t-cell activation by distinct mechanisms. *Molecular and cellular biology*, 25(21):9543–9553.

Pawelczyk, K., Piotrowska, A., Ciesielska, U., Jablonska, K., Glatzel-Plucinska, N., Grzegrzolka, J., Podhorska-Okolow, M., Dziegiel, P., and Nowinska, K. (2019). Role of pd-l1 expression in non-small cell lung cancer and their prognostic significance according to clinicopathological factors and diagnostic markers. *International journal of molecular sciences*, 20(4):824.

Philips, E. A., Garcia-España, A., Tocheva, A. S., Ahearn, I. M., Adam, K. R., Pan, R., Mor, A., and Kong, X.-P. (2020). The structural features that distinguish pd-l2 from pd-l1 emerged in placental mammals. *Journal of Biological Chemistry*, 295(14):4372–4380.

Ramos-Vara, J. and Miller, M. (2014). When tissue antigens and antibodies get along: revisiting the technical aspects of immunohistochemistry—the red, brown, and blue technique. *Veterinary pathology*, 51(1):42–87.

Rogge, R. A., Kalashnikova, A. A., Muthurajan, U. M., Porter-Goff, M. E., Luger, K., and Hansen, J. C. (2013). Assembly of nucleosomal arrays from recombinant core histones and nucleosome positioning dna. *JoVE (Journal of Visualized Experiments)*, (79):e50354.

Rudnizky, S., Bavly, A., Malik, O., Pnueli, L., Melamed, P., and Kaplan, A. (2016). H2a. z controls the stability and mobility of nucleosomes to regulate expression of the lh genes. *Nature communications*, 7(1):1–12.

Schats, K. A., Van Vré, E. A., Boeckx, C., De Bie, M., Schrijvers, D. M., Neyns, B., De Meester, I., and Kockx, M. M. (2018). Optimal evaluation of programmed death ligand-1 on tumor cells versus immune cells requires different detection methods. *Archives of pathology & laboratory medicine*, 142(8):982–991.

Sheppard, K.-A., Fitz, L. J., Lee, J. M., Benander, C., George, J. A., Wooters, J., Qiu, Y., Jussif, J. M., Carter, L. L., Wood, C. R., et al. (2004). Pd-1 inhibits t-cell receptor induced phosphorylation of the zap70/cd3ζ signalosome and downstream signaling to pkcθ. *FEBS letters*, 574(1-3):37–41.

Spiriti, J., Binder, J. K., Levitus, M., and Van Der Vaart, A. (2011). Cy3-dna stacking interactions strongly depend on the identity of the terminal basepair. *Biophysical journal*, 100(4):1049–1057.

Takaba, H. and Takayanagi, H. (2017). The mechanisms of t cell selection in the thymus. *Trends in immunology*, 38(11):805–816.

Takeuchi, M., Doi, T., Obayashi, K., Hirai, A., Yoneda, K., Tanaka, F., and Iwai, Y. (2018). Soluble pd-l1 with pd-1-binding capacity exists in the plasma of patients with non-small cell lung cancer. *Immunology letters*, 196:155–160.

Tang, L., Nogales, E., and Ciferri, C. (2010). Structure and function of swi/snf chromatin remodeling complexes and mechanistic implications for transcription. *Progress in biophysics and molecular biology*, 102(2-3):122–128.

Tang, S., Liao, J., and Long, Y. (2019). Comparative assessment of the efficacy of gross total versus subtotal total resection in patients with glioma: a meta-analysis. *International Journal of Surgery*, 63:90–97.

Taniguchi, K. and Karin, M. (2018). Nf-κb, inflammation, immunity and cancer: coming of age. *Nature Reviews Immunology*, 18(5):309–324.

Thiriet, C. and Hayes, J. J. (2001). A novel labeling technique reveals a function for histone h2a/h2b dimer tail domains in chromatin assembly in vivo. *Genes & development*, 15(16):2048–2053.

Thompson, R. H., Kuntz, S. M., Leibovich, B. C., Dong, H., Lohse, C. M., Webster, W. S., Sengupta, S., Frank, I., Parker, A. S., Zincke, H., et al. (2006). Tumor b7-h1 is associated with poor prognosis in renal cell carcinoma patients with long-term follow-up. *Cancer research*, 66(7):3381–3385.

Torlakovic, E., Lim, H. J., Adam, J., Barnes, P., Bigras, G., Chan, A. W., Cheung, C. C., Chung, J.-H., Couture, C., Fiset, P. O., et al. (2020). "interchangeability" of pd-l1 immunohistochemistry assays: a meta-analysis of diagnostic accuracy. *Modern Pathology*, 33(1):4–17.

Tsao, M. S., Kerr, K. M., Kockx, M., Beasley, M.-B., Borczuk, A. C., Botling, J., Bubendorf, L., Chirieac, L., Chen, G., Chou, T.-Y., et al. (2018). Pd-l1 immunohistochemistry comparability study in real-life clinical samples: results of blueprint phase 2 project. *Journal of Thoracic Oncology*, 13(9):1302–1311.

Viricel, C., Ahmed, M., and Barakat, K. (2015). Human pd-1 binds differently to its human ligands: a comprehensive modeling study. *Journal of Molecular Graphics and Modelling*, 57:131–142.

Voong, L. N., Xi, L., Wang, J.-P., and Wang, X. (2017). Genome-wide mapping of the nucleosome landscape by micrococcal nuclease and chemical mapping. *Trends in Genetics*, 33(8):495–507.

Wang, X., Teng, F., Kong, L., and Yu, J. (2016). Pd-l1 expression in human cancers and its association with clinical outcomes. *OncoTargets and therapy*, 9:5023.

Xue, S., Song, G., and Yu, J. (2017). The prognostic significance of pd-l1 expression in patients with glioma: A meta-analysis. *Scientific reports*, 7(1):1–8.

Yokosuka, T., Takamatsu, M., Kobayashi-Imanishi, W., Hashimoto-Tane, A., Azuma, M., and Saito, T. (2012). Programmed cell death 1 forms negative costimulatory microclusters that directly inhibit t cell receptor signaling by recruiting phosphatase shp2. *Journal of Experimental Medicine*, 209(6):1201–1217.

Zak, K. M., Kitel, R., Przetocka, S., Golik, P., Guzik, K., Musielak, B., Dömling, A., Dubin, G., and Holak, T. A. (2015). Structure of the complex of human programmed death 1, pd-1, and its ligand pd-l1. *Structure*, 23(12):2341–2348.

Appendix A

Appendix

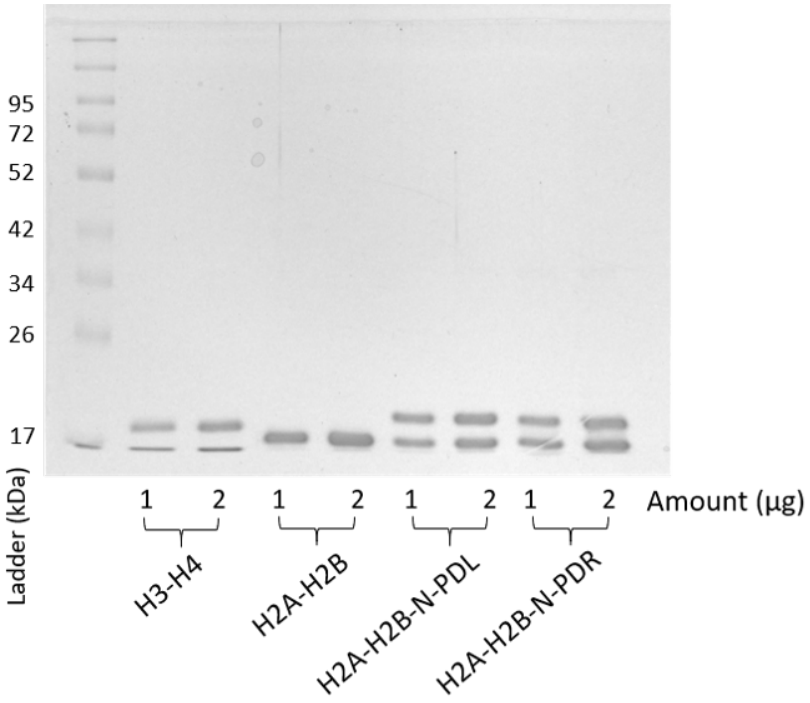

Figure A.1: Full Gel Image of Figure 3.7. In Figure 3.7, the H2A-H2B-N-PDL sample was omitted as this was not used for the experiments in this study. H2A-H2B-N-PDL, PD-L1 ligand peptide attached to the N-terminal of H2B.

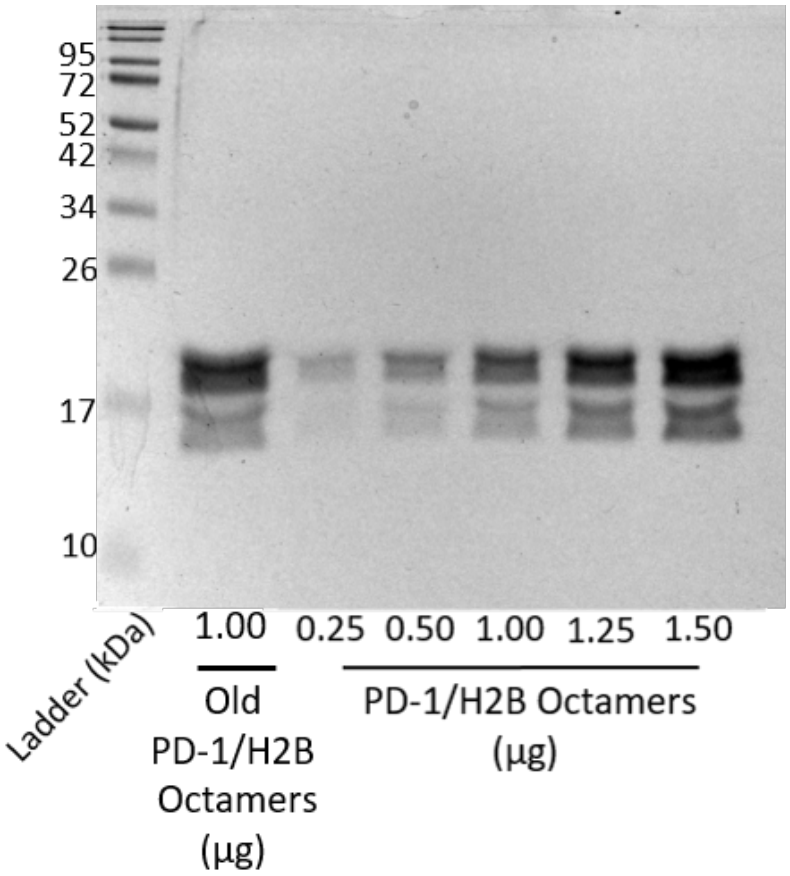

Figure A.2: Full Gel Image of Figure 3.9. In Figure 3.9, lanes indicating the previously made PD-1/H2B octamers were omitted to prevent confusion between them and the recently formed PD-1/H2B octamers. Previously formed PD-1/H2B histone octamers were purified and 1.00 µg was separated using 12% SDS-PAGE and stained with Coomassie blue.

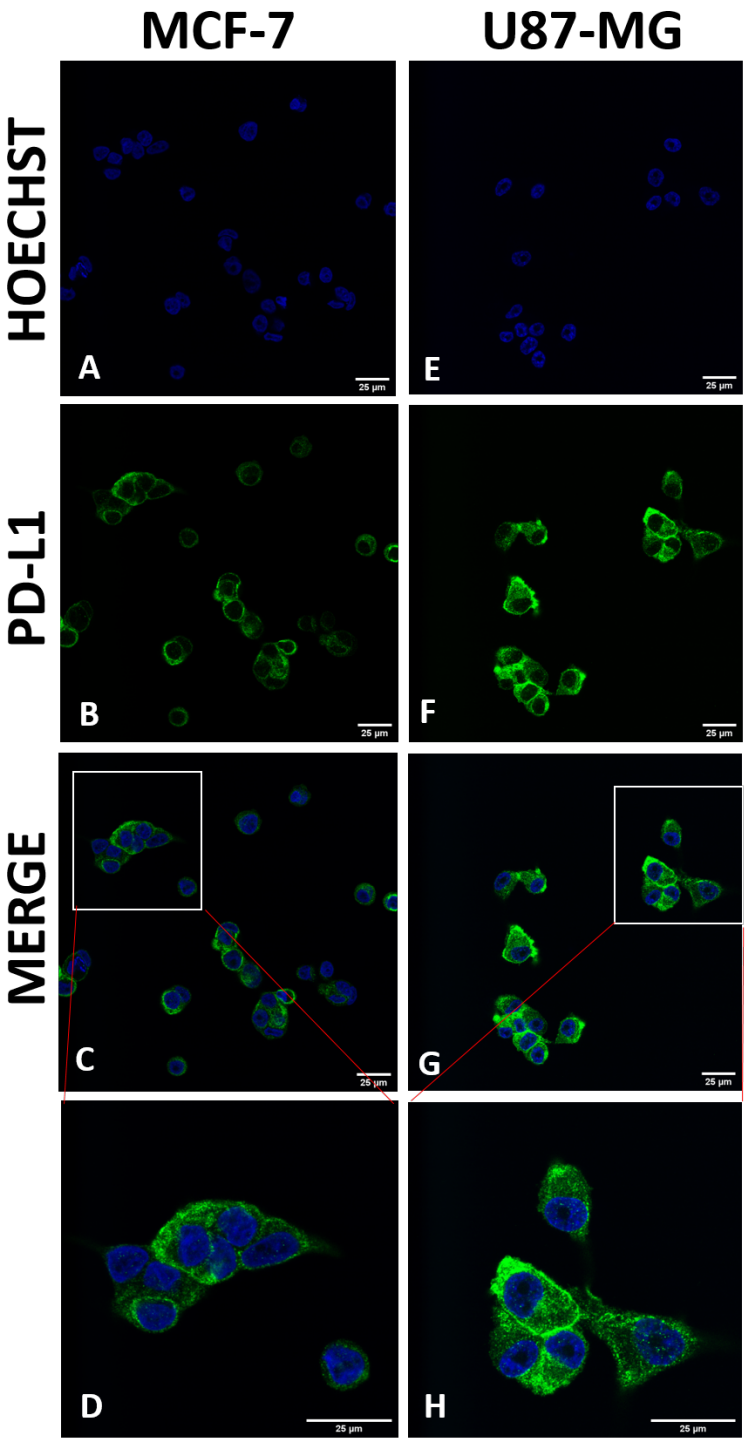

Figure A.3: MCF-7 and U87-MG Cells Express PD-L1 Differentially. MCF-7 cells (A-D) and U87-MG cells (E-H) were incubated with 2.85 µg/mL of PD-L1 antibody (green) overnight at 4°C with rocking, after which they were washed and incubated with anti-rabbit and 1 µg/mL of Hoechst 33342 (blue) to stain nuclear DNA, (D & H), representative cell magnified 2.5x of (C & G), scale bar: 25 µm.

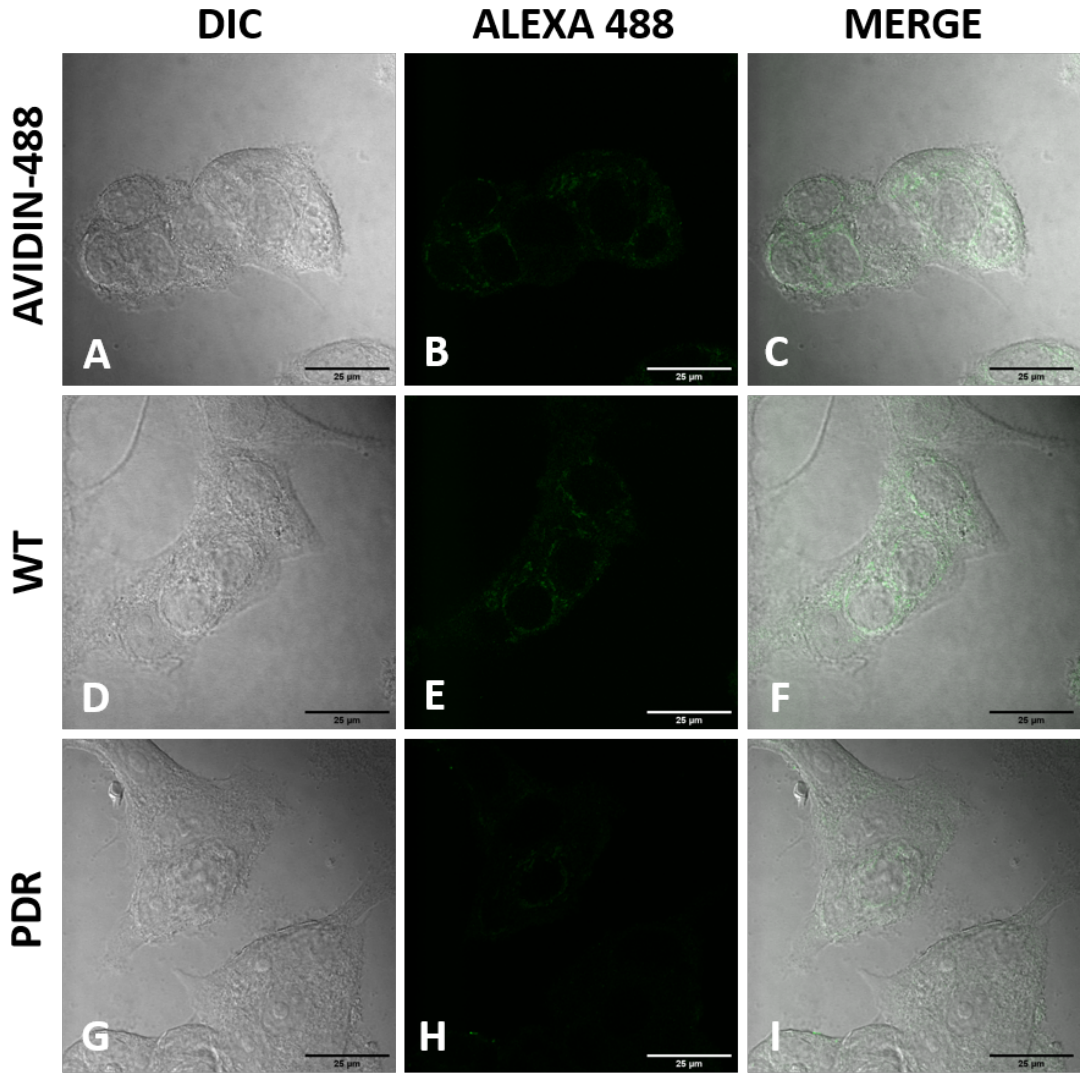

Figure A.4: Representative Images of PD-1/H2B Stained MCF-7 Cells. Fluorescence images of MCF-7 cells incubated with 2 µg of Avidin 488 conjugate, 1 µg of WT assembly, or 1 µg of PD-1/H2B nucleosomal array (PDR). After fixation and mounting, cells were imaged in brightfield DIC (left) and Avidin-488 was used to detect biotin-labelled nucleosomal array DNA. Merged images show PDR assembly as green, scale bar: µm.

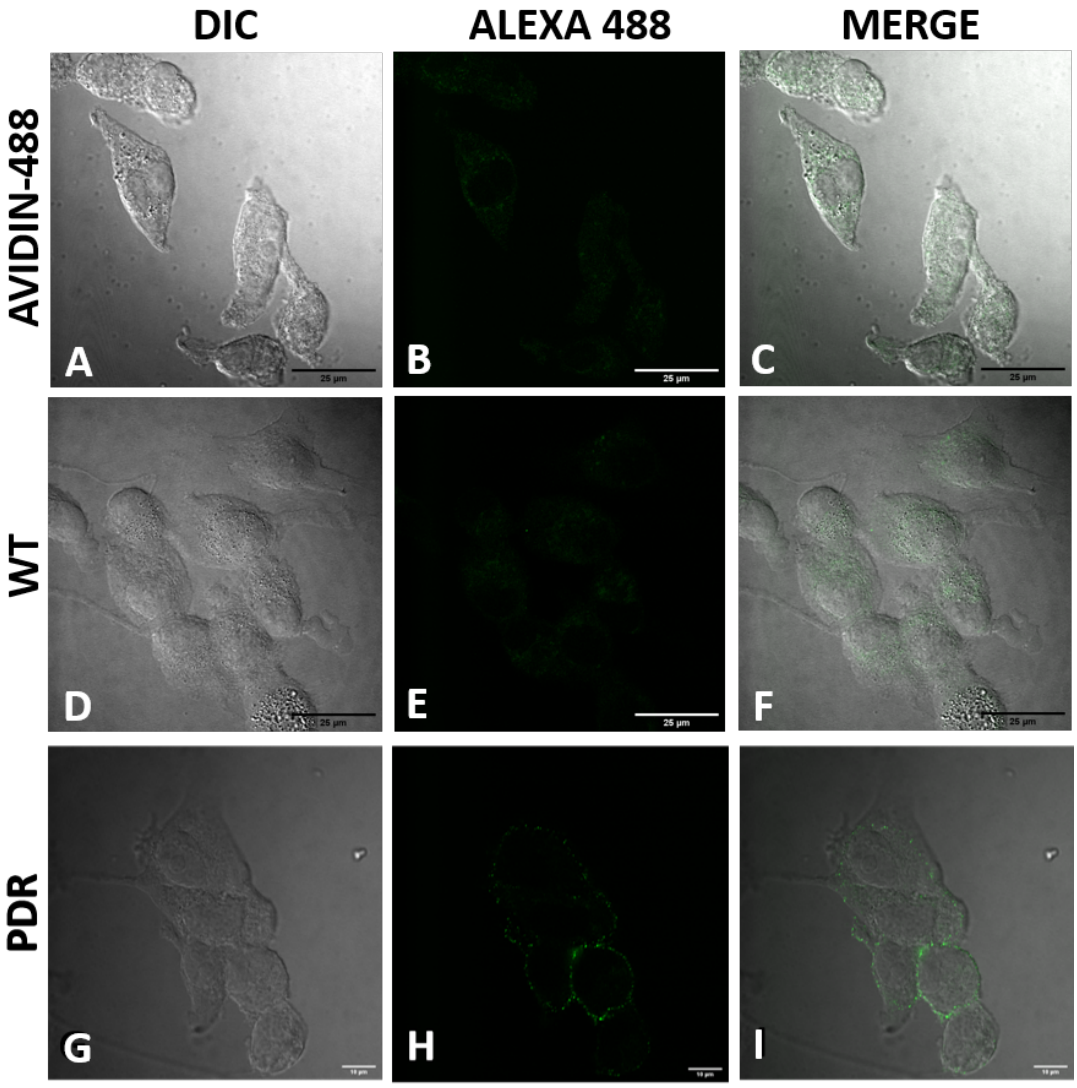

Figure A.5: Representative Images of PD-1/H2B Stained U87-MG Cells. Fluorescence images of U87-MG cells incubated with 2 µg of Avidin 488 conjugate, 1 µg of WT assembly, or 1 µg of PD-1/H2B nucleosomal array (PDR). After fixation and mounting, cells were imaged in brightfield DIC (left) and Avidin-488 was used to detect biotin-labelled nucleosomal array DNA. Merged images show PDR assembly as green, scale bar: µm.